Chapter 1
Kinetic Energy Harvesting

Dibin Zhu and Steve Beeby

Abstract This chapter introduces principles of normal kinetic energy harvesting and adaptive kinetic energy harvesting. Kinetic energy harvesters, also known as vibration power generators, are typically, although not exclusively, inertial spring-mass systems. Electrical power is extracted by employing one or a combination of different transduction mechanisms. Main transduction mechanisms are piezoelectric, electromagnetic and electrostatic. As most vibration power generators are resonant systems, they generate maximum power when the resonant frequency of the generator matches ambient vibration frequency. Any difference between these two frequencies can result in a significant decrease in generated power. Recent development in adaptive kinetic energy harvesting increases the operating frequency range of such generators. Possible solutions include tuning resonant frequency of the generator and widening the bandwidth of the generator. In this chapter, principles and operating strategies for adaptive kinetic energy harvesters will be presented and compared.

Keywords Adaptive energy harvesting · Frequency tuning · Wider frequency range · Vibration energy harvesting

1.1 Introduction

Mechanical energy can be found almost anywhere that wireless sensor networks (WSN) may potentially be deployed, which makes converting mechanical energy from ambient vibration into electrical energy an attractive approach for powering wireless sensors. The source of mechanical energy can be a moving human body or a vibrating structure. The frequency of the mechanical excitation depends on the source: less than 10 Hz for human movements and over 30 Hz for machinery

D. Zhu (✉)
School of Electronics and Computer Science, University of Southampton, Southampton, UK
e-mail: dz@ecs.soton.ac.uk

T.J. Kaźmierski, S. Beeby (eds.), *Energy Harvesting Systems*,
DOI 10.1007/978-1-4419-7566-9_1,

vibrations [1]. Such devices are known as kinetic energy harvesters or vibration power generators [2].

In practical machine-based applications, vibration levels can be very low (<1 m s^{-2}) at frequencies that often correspond to the frequency of the mains electricity powering the plant (e.g. 50 or 60 Hz or harmonics). Such low levels of vibration equate to amplitudes of vibration that are in the order of a few microns and the only way to extract mechanical energy in this case is to use an inertial generator that resonates at a characteristic frequency. The limitation to this approach is that the generator is, by definition, designed to work at a single frequency. A high Q-resonance means very limited practical bandwidths over which energy can be harvested. If the resonant frequency does not match the ambient vibration frequency, output power of the generator drops significantly.

Adaptive kinetic energy harvesters [3] are developed to increase the operational frequency range of vibration energy harvesters thus addressing the bandwidth limitation. Adaptive kinetic energy employs certain mechanisms that can either adjust, or tune, the resonant frequency of a single generator so that it matches the frequency of the ambient vibration at all times or widen the bandwidth of the generator. Resonant frequency tuning can be achieved by changing the mechanical characteristics of the structure or electrical load on the generator. In addition, widening the bandwidth of the generator can be achieved by, for example, employing an array of structures each with a different resonant frequency, an amplitude limiter, coupled oscillators, non-linear (e.g. magnetic) springs, bi-stable structures or a large inertial mass (large device size) with a high degree of damping.

In Section 1.2, principles of kinetic energy harvesting is introduced. In Section 1.3, classification of transduction mechanisms and principle of each transducer are described. A wide range of reported kinetic energy harvesters are summarized according to their transducers. Advantages and disadvantages of each transducer have been listed and compared. In Section 1.4, a brief introduction of adaptive kinetic energy harvesting is given. Section 1.5 describes the theory behind resonant frequency tuning strategies and suggests criteria for evaluating tuning mechanisms. Principles of the two tuning methods, i.e. mechanical and electrical tuning, are introduced and examples of these methods are studied. Section 1.6 presents principles of strategies to widen bandwidth of the kinetic energy harvesters and contains examples of all strategies. Section 1.7 compares different strategies for adaptive kinetic energy harvesting and Section 1.8 summarizes the chapter.

1.2 Principles of Kinetic Energy Harvesting

Inertial-based kinetic energy harvesters are modelled as second-order, spring-mass systems. The generic model of kinetic energy harvesters was first developed by Williams and Yates [4]. Figure 1.1 shows a generic model of such a generator, which consists of a seismic mass, m, and a spring with the spring constant of k. When the generator vibrates, the mass moves out of phase with the generator housing. There

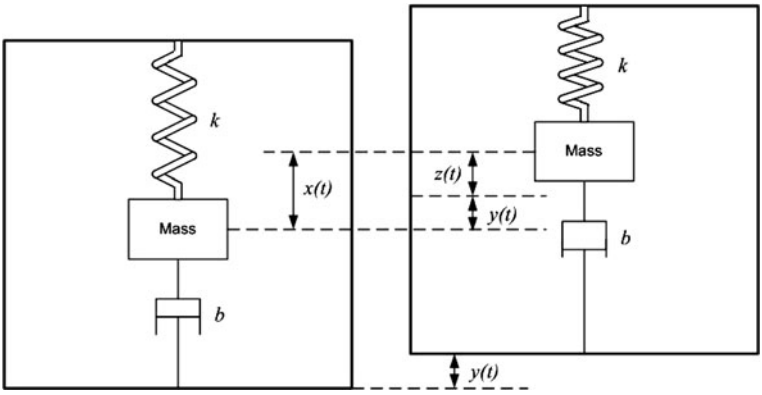

Fig. 1.1 Generic model of kinetic energy harvesters

is a relative movement between the mass and the housing. This displacement is sinusoidal in amplitude and can drive a suitable transducer to generate electrical energy. b is the damping coefficient that consists of mechanically induced damping (parasitic damping) coefficient b_{m} and electrically induced damping coefficient b_{e}, i.e. $b = b_{\mathrm{m}} + b_{\mathrm{e}}$. $y(t)$ is the displacement of the generator housing and $z(t)$ is the relative motion of the mass with respect to the housing. For a sinusoidal excitation, $y(t)$ can be written as $y(t) = Y \sin \omega t$, where Y is the amplitude of vibration and ω is the angular frequency of vibration.

The transduction mechanism itself can generate electricity by exploiting the mechanical strain or relative displacement occurring within the system. The strain effect utilizes the deformation within the mechanical system and typically employs active materials (e.g. piezoelectric). In the case of relative displacement, either the velocity or position can be coupled to a transduction mechanism. Velocity is typically associated with electromagnetic transduction while relative position is associated with electrostatic transduction. Each transduction mechanism exhibits different damping characteristics and this should be taken into consideration while modelling the generators. Thermomechanical system can be increased in complexity, for example, by including a hydraulic system to magnify amplitudes or forces, or couple linear displacements into rotary generators. Details of these transducers will be given in Section 1.3.

1.2.1 Transfer Function

For the analysis, it is assumed that the mass of the vibration source is much greater than the mass of seismic mass in the generator and the vibration source is unaffected by the movement of the generator. Then the differential equation of the movement of the mass with respect to the generator housing from the dynamic forces on the mass can be derived as follows:

$$m \cdot \frac{d^2 z\,(t)}{dt^2} + b \cdot \frac{dz\,(t)}{dt} + k \cdot z\,(t) = -m \cdot \frac{d^2 y\,(t)}{dt^2} \tag{1.1}$$

which can be written in the form after the Laplace transform as

$$m \cdot s^2 \cdot z(s) + b \cdot s \cdot z(s) + k \cdot s \cdot z(s) = -m \cdot a(s) \tag{1.2}$$

where $a(s)$ is the Laplace expression of the acceleration of the vibration, $a(t)$, which is given by

$$a(t) = \frac{d^2 y\,(t)}{dt^2} \tag{1.3}$$

Thus, the transfer function of a vibration-based micro-generator is

$$\frac{z(s)}{a(s)} = \frac{1}{s^2 + \frac{b}{m}s + \frac{k}{m}} = \frac{1}{s^2 + \frac{\omega_\mathrm{r}}{Q}s + \omega_\mathrm{r}^2} \tag{1.4}$$

where $Q = \frac{\sqrt{km}}{b}$ is the quality factor and $\omega_\mathrm{r} = \sqrt{k/m}$ is the resonant frequency.

1.2.2 Equivalent Circuit

An equivalent electrical circuit for a kinetic energy harvester can be found from Eq. (1.4), which, when rearranged, gives

$$-m \cdot a(s) = s \cdot Z(s)\left(ms + b + \frac{k}{s}\right) \tag{1.5}$$

Equation (1.5) can be rewritten as

$$-I(s) = E(s)\left(sC + \frac{1}{R} + \frac{1}{sL}\right) \tag{1.6}$$

where $I(s) = m \cdot a(s)$, $E(s) = s \cdot Z(s)$, $C = m$, $R = \frac{1}{b}$, $L = \frac{1}{k}$. Based on Eq. (1.6), an equivalent electrical circuit can be built as shown in Fig. 1.2.

1.2.3 Damping in Kinetic Energy Harvesters

As mentioned above, damping in kinetic energy harvesters consists of mechanically induced damping (parasitic damping) and electrically induced damping. The overall damping factor of the system, ζ_T, is given by

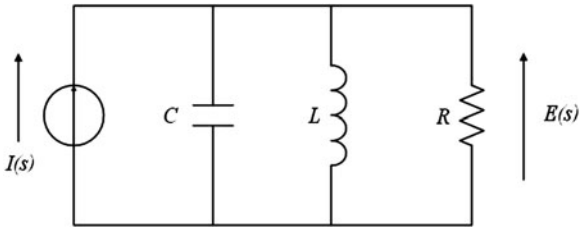

Fig. 1.2 Equivalent circuit of a kinetic energy harvester

$$\zeta_{\mathrm{T}} = \frac{b}{2m\omega_{\mathrm{r}}} = \frac{b_{\mathrm{m}} + b_{\mathrm{e}}}{2m\omega_{\mathrm{r}}} = \zeta_{\mathrm{m}} + \zeta_{\mathrm{e}} \tag{1.7}$$

where $\zeta_{\mathrm{m}} = \frac{b_{\mathrm{m}}}{2m\omega_{\mathrm{r}}}$ is the mechanically induced damping factor and $\zeta_{\mathrm{e}} = \frac{b_{\mathrm{e}}}{2m\omega_{\mathrm{r}}}$ is the electrically induced damping factor.

Total quality factor (Q-factor) is a function of damping factor. The total Q-factor is given by

$$Q_{\mathrm{T}} = \frac{1}{2\zeta_{\mathrm{T}}} \tag{1.8}$$

This is the Q-factor when the generator is connected to the optimum load. The relation between total quality factor and the electrical and mechanical damping is given by

$$\frac{1}{Q_{\mathrm{T}}} = \frac{1}{Q_{\mathrm{OC}}} + \frac{1}{Q_{\mathrm{e}}} \tag{1.9}$$

where $Q_{\mathrm{OC}} = \frac{1}{2\zeta_{\mathrm{m}}}$ is the open circuit Q-factor which reflects the mechanical damping. Q_{e}, which equals $\frac{1}{2\zeta_{\mathrm{e}}}$, reflects performance of the transduction mechanism. It cannot be measured directly, but can be calculated using Eq. (1.9) once Q_{T} and Q_{OC} are measured.

1.2.4 Output Power of Kinetic Energy Harvesters

Assume that the input is a sinusoid excitation, i.e. $y(t) = \sin \omega t$. The solution to Eq. (1.1) is given by

$$z(t) = \frac{m\omega^2 Y}{k - m\omega^2 + j\omega b} \cdot \sin \omega t \tag{1.10}$$

or

$$z(t) = \frac{\omega^2}{\sqrt{(\omega_r^2 - \omega^2)^2 + (\frac{b\omega}{m})^2}} \cdot Y \sin(\omega t + \varphi) \tag{1.11}$$

where φ is the phase angle given by

$$\varphi = \tan^{-1}\left(\frac{b\omega}{k - \omega^2 m}\right) \tag{1.12}$$

The average power dissipated within the damper, i.e. the sum of the power extracted by the transduction mechanism and the power lost in mechanical damping is given by

$$P = b\left(\frac{dz(t)}{dt}\right)^2 \tag{1.13}$$

Equations (1.11) and (1.13) give the average power dissipated within the damper as follows:

$$P(\omega) = \frac{m\zeta_T Y^2 (\frac{\omega}{\omega_r})^3 \omega^3}{[1 - (\frac{\omega}{\omega_r})^2]^2 + (2\zeta_T \frac{\omega}{\omega_r})^2} \tag{1.14}$$

When the generator is at resonance, i.e. $\omega = \omega_r$, the power dissipation reaches maximum. The maximum dissipated power is

$$P = \frac{mY^2\omega_r^3}{4\zeta_T} \tag{1.15}$$

or

$$P = \frac{mY^2\omega_r^3}{4(\zeta_m + \zeta_e)} \tag{1.16}$$

The power dissipation is the sum of maximum electrical energy extracted by the transduction mechanism, P_e, and mechanical loss, P_m. P_e and P_m are as follows:

$$P_e = \frac{\zeta_e mY^2\omega_r^3}{4(\zeta_m + \zeta_e)} \tag{1.17}$$

$$P_m = \frac{\zeta_m mY^2\omega_r^3}{4(\zeta_m + \zeta_e)} \tag{1.18}$$

Maximum power conversion from mechanical domain to electrical domain occurs when $\zeta_e = \zeta_m$, i.e. damping arising from the electrical domain equals mechanical losses. Therefore, the maximum electrical power that can be extracted by the kinetic energy harvester, P_e, is given by

$$P_e = \frac{P}{2} = \frac{mY^2\omega_r^3}{16\zeta_m} \tag{1.19}$$

Since the peak acceleration of the base, a, is given by $a = Y\omega^2$, Eq. (1.19) can be rewritten as

$$P_e = \frac{ma^2}{16\omega_r \cdot \zeta_m} \tag{1.20}$$

As the open circuit Q-factor, $Q_{OC} = \frac{1}{2\zeta_m}$, Eq. (1.20) can be written as

$$P_e = \frac{ma^2}{8\omega_r} \cdot Q_{OC} \tag{1.21}$$

It is found via Eq. (1.21) that the maximum power delivered to the electrical domain is inversely proportional to the damping factor, i.e. proportional to the Q-factor. Hence, when designing a vibration-based micro-generator to achieve maximum power output, it is important to design the generator with a high Q-factor (i.e. low damping factor) and make the generator work at its resonant frequency. Figure 1.3 shows an example of the power spectrum of a vibration-based micro-generator of resonant frequency 50 Hz with various Q-factors and damping factors. It can be seen that, for generators with a high Q-factor (i.e. low damping factor), the output power drops significantly if the frequency of operation is away from the generators resonance. When the Q-factor is lower (i.e. damping factor is higher), the peak output power decreases while the bandwidth of the generator increases and the device becomes less sensitive to frequency shifts at the expense of lower maximum generated power. In addition, since the output power is inversely proportional to the resonant frequency of the generator for a given acceleration, it is generally preferable to operate at the lowest available fundamental frequency. This is compounded by practical observations that acceleration levels associated with environmental vibrations tend to reduce with increasing frequency. Application vibration spectra should be carefully studied before designing the generator in order to correctly identify the frequency of operation given the design constraints on generator size and maximum permissible $z(t)$. Furthermore, the mass of the mechanical structure should be maximized within the given size constraints in order to maximize the electrical power output. It should also be noted that the energy delivered to the electrical domain will not necessarily all be usefully harvested (e.g. coil losses).

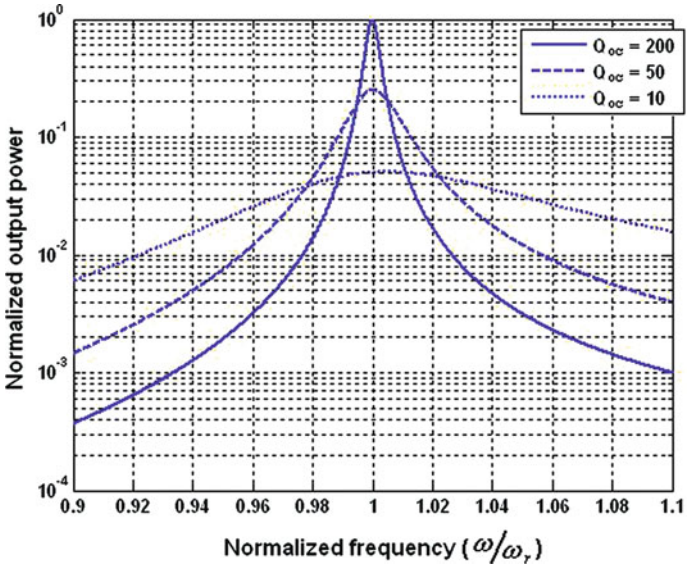

Fig. 1.3 Power spectrum of a kinetic energy harvester with various Q-factors

1.3 Transduction Mechanisms

In kinetic energy harvesting, a particular transduction mechanism such as electromagnetic [5], electrostatic [6] and piezoelectric [7] is used to extract electrical energy from motion. The generator also requires a mechanical system to couple environmental displacements to the transduction mechanism. This mechanical system has to be designed to maximize the coupling between the mechanical energy source and the transduction mechanism. Most vibration-based micro-generators are single degree of freedom second-order spring-mass system consisting of an inertial frame that transmits the vibration to a suspended inertial mass to produce a relative displacement or cause mechanical strain. The transduction mechanism can then generate electrical energy by exploiting the relative displacement or strain.

1.3.1 Electromagnetic (EM) Generators

Electromagnetic induction was discovered by Michael Faraday in 1831. Faraday's law of electromagnetic induction states that an electrical current will be induced in any closed circuit when the magnetic flux through a surface bounded by the conductor changes. This applies whether the field itself changes in strength or the conductor is moved through it. In an electromagnetic generator, permanent magnets are used to produce strong magnetic field and a coil is used as the conductor. Either the permanent magnet or the coil is fixed to the frame while the other is attached to the inertial mass. The relative displacement caused by the vibration makes the

transduction mechanism work and generate electrical energy. The induced voltage, also known as electromotive force (e.m.f), across the coil is proportional to the strength of the magnetic field, the velocity of the relative motion and the number of turns of the coil. An electromagnetic generator is characterized by high output current level at the expense of low voltages. Figure 1.4 shows two commonly seen examples of electromagnetic generators.

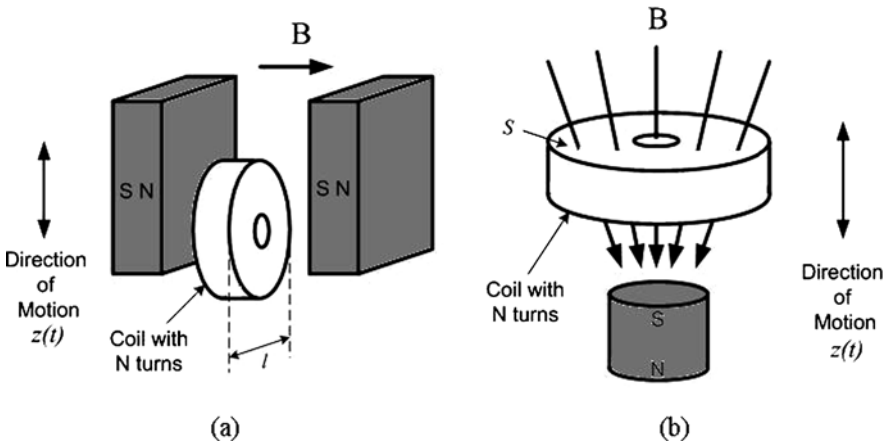

Fig. 1.4 Electromagnetic generators

For the case in Fig. 1.4a, the magnetic field is uniform. The magnetic field cut by the coil varies with the relative displacement between magnets and the coil. In this case, the induced electromotive force is given by

$$\text{e.m.f.} = -N \cdot l \cdot B \cdot \frac{dz}{dt} \tag{1.22}$$

where N is the number of turns of the coil, l is the effective length of the coil, B is the flux density going through the coil and dz/dt is the relative velocity between the magnets and the coil.

For the case in Fig. 1.4b, the magnetic field varies with the distance apart from the magnet. The induced electromotive force is given by

$$\text{e.m.f.} = -N \cdot S \cdot \frac{dB}{dz} \cdot \frac{dz}{dt} \tag{1.23}$$

where S is the effective area of the coil and dB/dz is the gradient of the magnetic flux density along the direction of relative motion between magnets and the coil.

In both cases, the induced e.m.f. is a function of velocity of relative movement $z(t)$. Therefore, both expressions can be expressed by

$$\text{e.m.f.} = \kappa \cdot \frac{dz}{dt} \tag{1.24}$$

where κ is the electromagnetic coupling factor which equals $-N \cdot l \cdot B$ and $-N \cdot S \cdot \frac{dB}{dz}$ in both cases, respectively. It represents the change in coupled flux per unit displacement.

Figure 1.5 shows a circuit representation of an electromagnetic generator with a resistive load, R_L. The relation between the current through the load and the induced e.m.f. is given by

$$\text{e.m.f.} + i \cdot (R_\text{L} + R_\text{c}) + L_\text{c} \frac{di}{dt} = 0 \tag{1.25}$$

Electromagnetic generators perform better in macro-scale than in micro-scale [8]. Particularly, generators integrated with MEMS with electroplated coils and magnets may not be able to produce useful power levels due to poor electromagnetic coupling.

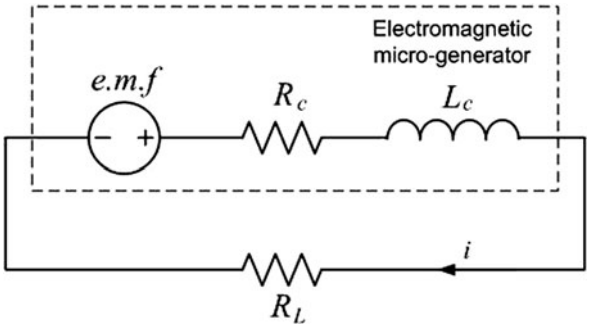

Fig. 1.5 Circuit representation of an electromagnetic generator

The damping coefficient induced from electromagnetic transduction, b_e, is as follows:

$$b_\text{e} = \frac{\kappa^2}{R_\text{L} + R_\text{c} + j\omega L_\text{c}} \tag{1.26}$$

where R_L and R_c are resistances of the load and coil, respectively. L_c is the inductance of the coil.

For a micro-generator that works at low resonant frequencies, the inductive impedance of the coil is much lower than its resistive impedance. Hence, the inductive impedance can be ignored in this case. Thus, b_e, can be simplified to

$$b_e = \frac{\kappa^2}{R_L + R_c} \tag{1.27}$$

The electrically induced damping factor, ζ_e, is

$$\zeta_e = \frac{\kappa^2}{2m\omega(R_L + R_c)} \tag{1.28}$$

Equation (1.28) shows that R_L can be used to adjust b_e to match b_m and therefore maximize output power, although this must be done with the coil parameters in mind. It can be shown that the optimum load resistance can be found from Eq. (1.29) and maximum average power delivered to the load can be found from Eq. (1.30) [9]:

$$R_L = R_c + \frac{\kappa^2}{b_m} \tag{1.29}$$

$$P_e = \frac{ma^2}{16\zeta_m\omega_r(1 - \frac{R_c}{R_L})} \tag{1.30}$$

Table 1.1 lists some reported electromagnetic generators with their main characteristics.

Table 1.1 Summary of electromagnetic kinetic energy harvesters

Reference	f (Hz)	Excitation level (m s^2)	Mass (g)	Volume (mm^3)	P (μW)	Power density (μW mm^3)	Structure material
Williams et al. [10]	4400	382	0.0023	5.4	0.3	0.0556	GaAs Polyimide[b]
Ching et al. [11]	110	95.5	N/A	1000	830	0.83	Copper[c]
Glynne-Jones et al. [12]	322	2.7	N/A	840	180	0.214	Steel[c]
Koukharenko et al. [13]	1615	3.92	N/A	100	0.104	0.00104	Silicon[b]
Saha et al. [14]	84	7.8	25	800[a]	3500	4.375	Copper[c]
Beeby et al. [15]	52	0.589	0.66	150	46	0.307	BeCu[c]
Klahand et al. [16]	25	N/A	15.6[a]	2000[a]	3.97	0.00199	Styrene[b]
Torah et al. [17]	50	0.589	N/A	570	58	0.102	BeCu[c]
Wang et al. [18]	280	10	N/A	315	17.2	0.055	Nickel[b]

[a] Estimated or extrapolated from data in reference
[b] Micro-scale
[c] Macro-scale

1.3.2 Piezoelectric (PZ) Generators

The piezoelectric effect was discovered by Pierre and Jacques Curie in 1880. It is the ability of some materials (notably crystals and certain ceramics) to generate an electric potential in response to applied mechanical stress. The electrical polarization is proportional to the applied strain. This is the piezoelectric effect used for mechanical to electrical energy conversion. Commonly used materials for piezoelectric power generation are PZT, PVDF [19] and macro-fibre composite (MFC) [20].

Piezoelectric generators typically work in either 33 mode (Fig. 1.6a) or 31 mode (Fig. 1.6b). In the 33 mode, a force is applied in the same direction as the poling direction, such as the compression of a piezoelectric block that has electrodes on its top and bottom surfaces. In the 31 mode, a lateral force is applied in the direction perpendicular to the poling direction, an example of which is a bending beam that has electrodes on its top and bottom surfaces. Generally, the 31 mode has been the most commonly used coupling mode although the 31 mode has a lower coupling coefficient than the 33 mode [19]. Common energy harvesting structures such as cantilevers or double-clamped beam typically work in the 31 mode because the lateral stress on the beam surface is easily coupled to piezoelectric materials deposited onto the beam.

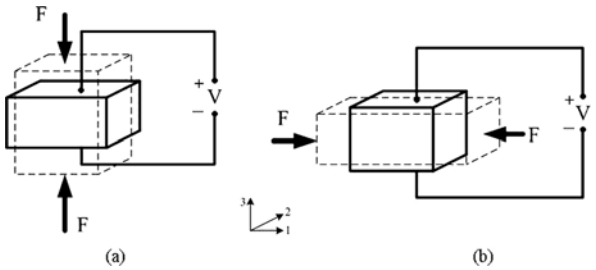

Fig. 1.6 Piezoelectric generators: (**a**) 33 mode and (**b**) 31 mode

The constitutive equations for a piezoelectric material are given by

$$\delta = \frac{\sigma}{Y} + d \cdot E \tag{1.31}$$

$$D = \varepsilon \cdot E + d \cdot \sigma \tag{1.32}$$

where δ is mechanical strain, σ is mechanical stress, Y is Young's modulus of the material, d is the piezoelectric strain coefficient, E is the electric field, D is the electrical displacement (charge density) and ε is the dielectric constant of the piezoelectric material.

Figure 1.7 shows a circuit representation of a piezoelectric generator with a resistive load, R_L. C is the capacitance between two electrodes and R_s is the resistance

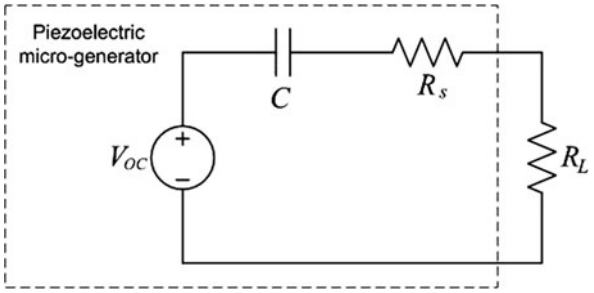

Fig. 1.7 Circuit representation of a piezoelectric generator

of the piezoelectric material. The voltage source, V_{OC}, is the open circuit voltage resulting from Eq. (1.32) when the electrical displacement is zero. It is given by

$$V_{\mathrm{OC}} = -\frac{d \cdot t}{\varepsilon} \cdot \sigma \tag{1.33}$$

where t is the thickness of the piezoelectric material.

An expression for the piezoelectric damping coefficient is [21]

$$b_{\mathrm{e}} = \frac{2m\omega_{\mathrm{r}}^2\kappa^2}{2\sqrt{\omega_{\mathrm{r}}^2 + \frac{1}{R_{\mathrm{L}}C_{\mathrm{L}}}}} \tag{1.34}$$

where κ is the piezoelectric material electromechanical coupling factor and C_{L} is the load capacitance. Again R_{L} can be used to optimize and the optimum value can be found from Eq. (1.35) and as stated previously, maximum power occurs when ζ_{e} equals ζ_{m}:

$$R_{\mathrm{opt}} = \frac{1}{\omega_{\mathrm{r}}C}\frac{2\zeta_{\mathrm{m}}}{\sqrt{4\zeta_{\mathrm{m}}^2 + \kappa^4}} \tag{1.35}$$

The maximum power is [21]

$$P_{\max} = \frac{1}{\omega_{\mathrm{r}}^2}\frac{R_{\mathrm{L}}C^2(\frac{2Ydtb^*}{\varepsilon})^2}{(4\zeta_{\mathrm{m}}^2 + \kappa^4)(R_{\mathrm{L}}C\omega_{\mathrm{r}})^2 + 4\zeta_{\mathrm{m}}\kappa^2(R_{\mathrm{L}}C\omega_{\mathrm{r}}) + 2\zeta_{\mathrm{m}}^2}a^2 \tag{1.36}$$

where b^* is a constant related to dimensions of the piezoelectric generator and a is the vibration acceleration.

Table 1.2 lists properties of some common piezoelectric materials. Output power of piezoelectric generators using different piezoelectric materials is compared in

Table 1.2 Coefficients of common piezoelectric materials [2, 22]

Material	PZT-5H	PZT-5A	$BaTiO_3$	PVDF
d_{31} ($\times 10^{-12} CN^{-1}$)	−274	−171	78	23
Young's modulus (GPa)	50	50	67	2
Relative permittivity ($\varepsilon/\varepsilon_0$)	3400	1700	1700	12

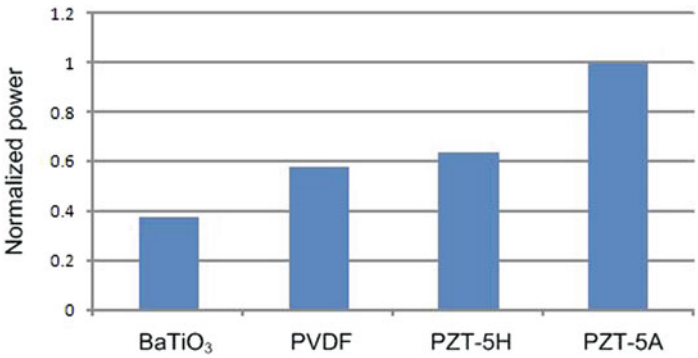

Fig. 1.8 Comparison of output power of piezoelectric generator using different piezoelectric materials

Fig. 1.8. These generators have the same dimensions. It is found that with the same dimensions, the generator using PZT-5A has the most amount of output power.

Piezoelectric generators have the simplest structure among the three transducers and they can produce appropriate voltages for electronic devices. However, the mechanical properties of the piezoelectric material may limit overall performance and lifespan of the generator. Although piezoelectric thin films can be integrated into a MEMS fabrication process, the piezoelectric coupling is greatly reduced. Therefore, the potential for integration with microelectronics is less than that for electrostatic micro-generators which will be presented in the next section.

Table 1.3 lists some reported piezoelectric generators with their main characteristics.

1.3.3 Electrostatic (ES) Generators

The basis of electrostatic generator is the variable capacitor. The variable capacitance structure is driven by mechanical vibrations. The capacitance varies between maximum and minimum values. If the charge on the capacitor is constrained, charge will move from the capacitor to a storage device or to the load as the capacitance decreases. Thus, mechanical energy is converted to electrical energy. Electrostatic generators can be classified into three types, i.e. in-plane overlap (Fig. 1.9a) which varies the overlap area between electrode fingers, in-plane gap closing (Fig. 1.9b) which varies the gap between electrode fingers and out-of-plane gap closing (Fig. 1.9c) which varies the gap between two large electrode plates [6].

Table 1.3 Summary of piezoelectric kinetic energy harvesters

Reference	f (Hz)	Excitation level (m s^2)	Mass (g)	Volume (mm^3)	P (μW)	Power density (μW mm^3)	Structure	Piezoelectric material
White et al. [23]	80	2.3	0.8	125	2.1	0.0168	Unimorph	Screen-printed PZT
Roundy et al. [1]	120	2.5	9.2	1000	375	0.375	Bimorph	PZT
Lu et al. [24]	7000	N/A	N/A	N/A	1600[a]	N/A	Bimorph	PZT-PIC255
Jeon et al. [25]	13.9	106	N/A	0.027[b]	1	37.04	Unimorph	PZT
Fang et al. [26]	608	9.8	0.0016[b]	0.6[b]	2.16	3.6	Unimorph	PZT
Marzencki et al. [27]	1500	3.92	0.0009[b]	5	0.03	0.006	Unimorph	AlN
Jeong et al. [28]	120	0.98	N/A	N/A	500	22	Bimorph	PMNZT
Kok et al. [29]	230	9.8	N/A	N/A	0.27	N/A	Free-standing unimorph	PZT
Shen et al. [30]	462.5	19.6	N/A	N/A	2.15	3.3	Unimorph	PZT
Zhu et al. [31]	67	4	2.8	987	240	0.24	Bimorph	Screen-printed PZT

[a] Simulation result
[b] Extrapolated from data in reference

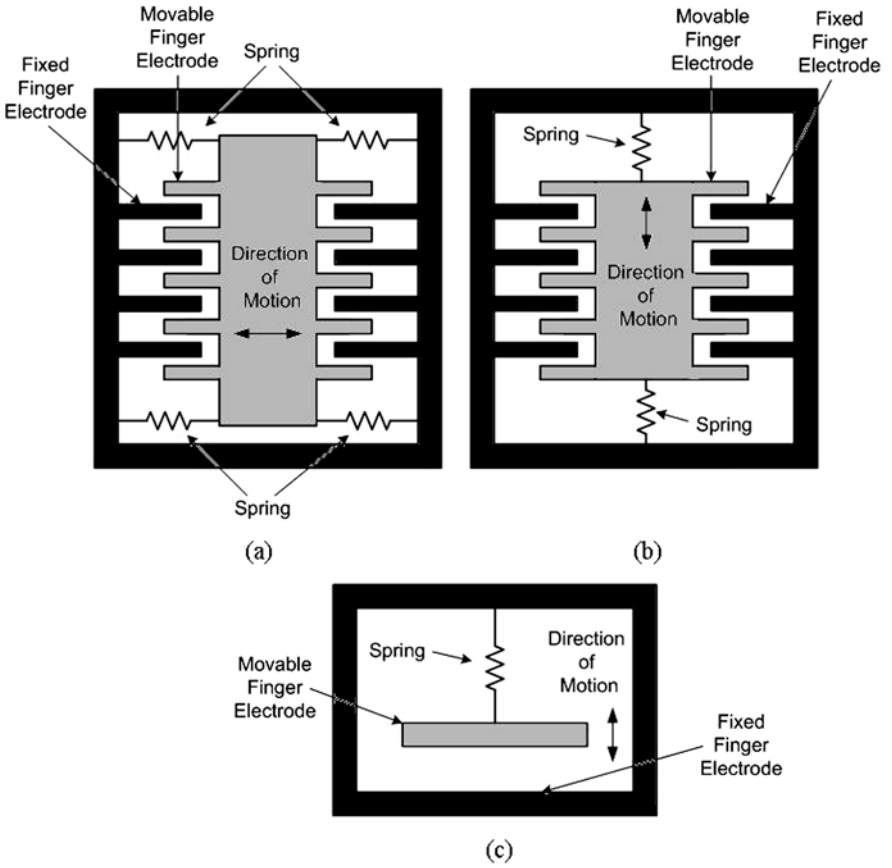

Fig. 1.9 Electrostatic generators: (**a**) in-plane overlap; (**b**) in-plane gap closing; and (**c**) out-of-plane gap closing

These three types can be operated either in charge-constrained or voltage-constrained cycles. Generally, generators working in voltage-constrained cycles provide more energy than generators in charge-constrained cycles. However, by incorporating a capacitor in parallel with the energy harvesting capacitor, the energy from the charge-constrained system can approach that of the voltage-constrained system as the parallel capacitance approaches infinity. This parallel capacitor effectively constrains the voltage on the energy harvesting capacitor [32].

A simplified circuit for an electrostatic generator using charge-constrained conversion is shown in Fig. 1.10. V_{in} is a pre-charged reservoir, which could be a capacitor or a rechargeable battery. C_{v} is a variable capacitor, which is one of the three types mentioned above. C_{par} is the parasitic capacitance associated with the variable capacitor structure and any interconnections, which limits the maximum voltage. C_{L} is the storage capacitor or any kind of load.

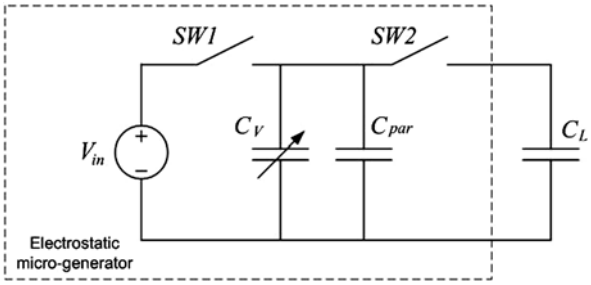

Fig. 1.10 Circuit representation for an electrostatic generator

The maximum voltage across the load is given by:

$$V_{\max} = \frac{C_{\max} + C_{\text{par}}}{C_{\min} + C_{\text{par}}} V_{\text{in}} \tag{1.37}$$

The energy dissipated within the damper, and therefore the power, is given by the force distance product shown in Eq. (1.37) [33]:

$$P = \frac{4YF\omega\omega_{\text{c}}^2}{2\pi} \sqrt{\frac{1}{1-\omega_{\text{c}}^2} - \left(\frac{F}{mY\omega^2\omega_{\text{c}}} U\right)^2} \tag{1.38}$$

where F is the damping force and Y is the displacement of the frame, $\omega_{\text{c}} = \omega/\omega_{\text{r}}$ and $U = \frac{\sin(\pi/\omega_{\text{c}})}{1+\cos\pi/\omega_{\text{c}}}$.

The optimum damping force is given by

$$F_{\text{opt}} = \frac{Y\omega^2 m}{\sqrt{2}} \frac{\omega_{\text{c}}}{|(1-\omega_{\text{c}}^2)U|} \tag{1.39}$$

An electrostatic generator can be easily realized in MEMS version. Since the fabrication process of electrostatic generators is similar to that of VLSI, electrostatic generators can be assembled with VLSI without difficulties. Unfortunately, electrostatic generators require an initial polarizing voltage or charge. The output impedance of the devices is often very high, which makes them less suitable as a power supply. However, they can be used to charge a battery, in which case, electrostatic generators can use electrets to provide the initial charge.

Table 1.4 lists some reported electrostatic generators with their main characteristics.

Table 1.4 Summary of electrostatic kinetic energy harvesters

Reference	f (Hz)	Excitation level (m s^2)	Mass (g)	Volume (mm^3)	P (μW)	Power density (μW mm^3)	Type
Meninger et al. [34]	2520	N/A	N/A	75	8	0.11	IPO
Tashiro et al. [35]	6	1	780	N/A	36	N/A	OP
Mitcheson et al. [36]	30	50	0.1	750	3.7	0.0049	N/A
Arakawa et al. [37]	10	3.9	N/A	800	6	0.0075	IPO
Despesse et al. [38]	50	8.8	104	1800	1052	0.584	IPGC
Kuehne et al. [39]	1000	1.96	N/A	N/A	4.28	0.079	IPO
Yen et al. [40]	1560	82.32	N/A	N/A	1.8	N/A	OP
Sterken et al. [41]	500	9.8	N/A	N/A	5	N/A	OP
Lo and Tai [42]	50	576.6	54	50,000	17.98	0.00036	OP
Hoffmann et al. [43]	1300–1500	127.4	642e-6	N/A	3.5	N/A	IPO
Naruse et al. [44]	2	3.92	N/A	N/A	40	N/A	IPGC

IPO in-plane overlap, *IPGC* in-plane gap closing, *OP* out-of-plane

1.3.4 Other Transduction Mechanisms

Magnetostrictive materials are also used to extract electrical energy from ambient vibration. These materials deform when placed in a magnetic field and it can induce changes in magnetic field when it is strained. Magnetostrictive materials are generally used in piezoelectric-magnetostrictive composites. Such composites were originally used in magnetic field sensors and have recently been adopted in energy harvesting.

Huang et al. [45] reported two energy harvesting devices based on a Terfenol-D/PZT/Terfenol-D composite. Their device produced 1.2 mW of power when excited at 5 m s^{-2} at 30 Hz. Recently, Wang and Yuan [46] reported a new vibration energy harvester based on magnetostrictive material, Metglas 2605SC, with electromagnetic pickup. Experimentally, the maximum output power and power density on the load resistor can reach 200 μW and 900 μW cm^{-3}, respectively, at a low frequency of 58 Hz. For a working prototype under a vibration with resonance frequency of 1.1 kHz and peak acceleration of 8.06 m s^{-2}, the average power and power density during charging the ultracapacitor can achieve 576 μW and 606 μW cm^{-3}, respectively. Dai et al. [47] reported an energy harvester that converts ambient mechanical vibration into electrical energy employing the Terfenol-D/PZT/Terfenol-D laminate magnetoelectric (ME) transducer. The har-

vester uses four magnets arranged on the free end of a cantilever beam. The magnets produce a concentrated flux gradient in the air gap, and the ME transducer is placed in the air gap between the magnets. When the harvester is excited, the magnetic circuit moves relative to the ME transducer. The experimental results showed that the generator produced a power of 2.11 mW for an acceleration of 9.8 m s^{-2} at a resonant frequency of 51 Hz.

1.3.5 Comparisons of Transduction Mechanisms

The efficiency of a generator should be simply defined by the standard definition, $\eta = E_{\text{out}}/E_{\text{in}}$, where E_{out} is the energy delivered to an electrical load and E_{in} is the input energy from the excitation vibrations per cycle. Roundy [48] has proposed a method based upon a standard two-port model of a transducer which enables the different transduction mechanisms to be compared. The analysis uses a coupling coefficient, κ, which is a measure of the efficiency of the conversion from the external vibration energy to the energy stored within the generator and transmission coefficient, λ, which is mathematically identical to the equation for efficiency given above. The transmission coefficient is related to the coupling coefficient and λ_{max} can be found from

$$\lambda_{\text{max}} = \frac{\kappa^2}{4 - 2\kappa^2} \tag{1.40}$$

In practice the transmission coefficient depends upon the load resistance which should be chosen to achieve λ_{max}. The maximum power can be found from Eq. (1.41) where ω is the circular frequency of driving vibrations:

$$P_{\text{max}} = \lambda_{\text{max}} \omega E_{\text{in}} \tag{1.41}$$

These coefficients have been derived by Roundy for each of the transduction mechanisms and can be employed to compare them as follows. In the case of the electromagnetic generator, the coupling factor is given in Section 1.3.1. For piezoelectric generators, the following equation applies where d is the piezoelectric strain coefficient (see Section 1.3.2), Y is Young's modulus and ε is the dielectric constant:

$$\kappa^2 = \frac{d^2 Y}{\varepsilon} \tag{1.42}$$

The maximum energy density for both electromagnetic and piezoelectric generators is given by

$$p_{\max} = \frac{\kappa^2 \rho (Q \cdot a)^2}{4\omega} \tag{1.43}$$

where ρ is the density of the proof mass material, Q is the quality factor of the generator and a is the magnitude of acceleration of the excitation vibrations.

The maximum energy density for electrostatic generators is non-linear and depends upon the geometry and operating conditions of the device. Taking the example of an out-of-plane parallel plate capacitor operating in a constant charge mode as described in Section 1.3.3.

$$\kappa^2 = \frac{V_{\text{in}}^2 C_{\max}^2}{V_{\text{in}}^2 C_{\max}^2 + m\omega^2 z^2 C(z)} \tag{1.44}$$

Equation (1.44) gives the coupling coefficient where V_{in} is the input voltage, z the displacement of the top electrode and $C_{\max}$ is the maximum capacitance. It is clear that the capacitance varies with displacement and therefore the coupling coefficient varies throughout the cycle. The average power output density is given by Eq. (1.45) where f is the generator frequency in hertz:

$$p_{\text{ave}} = f \frac{\rho (Q \cdot a)^2}{4\omega^2} \int_{t1}^{t2} \kappa(t) dt \tag{1.45}$$

The coupling coefficient of piezoelectric generators depends mainly on the piezoelectric material used, although the elastic properties of the other materials used in the generator structure may also influence the values. The coupling coefficient of electromagnetic generators is dependant upon the magnetic circuit of the device. In the case of electrostatic generators the coupling coefficient varies with position and device design.

Advantages and disadvantages of each type of transduction mechanism are summarized in Table 1.5.

Since electrostatic and piezoelectric transducers are compatible with MEMS, they are more suitable to be deployed in micro- or nano-scale systems while electromagnetic and magnetostrictive transducers are suitable for macro-scale systems. Roundy et al. [21] calculated the theoretical maximum energy density of the first three transducers. It was concluded that piezoelectric and electromagnetic transducers have similar energy density which is about 10 times that of electrostatic transducers.

Table 1.6 lists some commercially available vibration-based micro-generators. To the date, only generators with electromagnetic and piezoelectric transducers can

Table 1.5 Comparisons of different transduction mechanisms of kinetic energy harvesters

Type	Advantages	Disadvantages
Electromagnetic	• No external voltage source • No mechanical constraints needed • High output current	• Difficult to integrate with MEMS fabrication process • Poor performance in micro-scale • Low output voltage
Piezoelectric	• Simple structure • No external voltage source • Compatible with MEMS • High output voltage • No mechanical constraints needed	• Thin films have poor coupling • Poor mechanical properties • High output impedance • Charge leakage • Low output current
Electrostatic	• Easy to integrate with MEMS fabrication process • High output voltage	• Mechanical constraints needed • External voltage source or pre-charged electret needed • High output impedance • Low output current
Magnetostrictive	• Ultra-high coupling coefficient • High flexibility	• Non-linear effect • May need bias magnets • Difficult to integrate with MEMS fabrication process

Table 1.6 Summary of kinetic energy harvesters available on the market

Model	f (Hz)	Excitation level (m s^{-2})	Total mass (g)	Volume (mm^3)		P (mW)	Transducer
Mide Technology Corporation [49]							
Volture PEH20w	80–175[a]	13.7	85.14	39,963[b]	388.55[c]	2–24	PZ
Volture PEH25w	50–140[a]	13.7	85.14	40,543[b]	194.27[c]	2.5–24	PZ
Perpetuum Ltd. [50]							
PMG-17	100/120	9.8	655	522,682[b]		45	EM
PMG-27	17.2	0.49	400	467,711[b]		4	EM

PZ Piezoelectric, *EM* Electromagnetic

[a] Tunable by changing the length of the cantilever manually

[b] Total device

[c] Piezo wafer

be found on the market, which indicates that these two transducers are more feasible in practice.

1.4 Introduction to Adaptive Kinetic Energy Harvesting

Mathematical analysis presented in Section 1.2 showed that maximum power is generated when the resonant frequency of the generator matches the frequency of the ambient vibration. The limitation to this feature is that the generator is, by definition, designed to work at a single frequency. A high Q-resonance means very limited practical bandwidths over which energy can be harvested. If the resonant frequency of the generator does not match the ambient vibration frequency, the generated power drops dramatically. Most reported kinetic energy harvesters are designed to work only at one particular frequency [2]. For applications such as moving vehicles, human movement and wind-induced vibration where the frequency of ambient vibration changes occasionally, the efficiency of generators with one fixed resonant frequency is significantly reduced since the generator will not always be at resonance. This drawback must be overcome if kinetic energy harvesters are to be widely applicable in powering wireless systems. Therefore, adaptive energy harvesting is developed to increase operational frequency range of kinetic energy harvesters. To date, there are, in general, two approaches to achieving adaptive energy harvesters.

The first approach is to adjust, or tune, the resonant frequency of a single generator so that it matches the frequency of the ambient vibration at all times. This can be achieved by changing the mechanical characteristics of the structure or electrical load of the generator. Resonant frequency tuning methods can be classified as intermittent and continuous tuning [3]. Intermittent tuning is defined as a tuning mechanism that operates periodically. This approach only consumes power during the tuning operation and uses negligible energy once the generator is matched to the frequency of the ambient vibrations. Continuous tuning is defined as a tuning mechanism that is continuously applied even if the resonant frequency equals the ambient vibration frequency. The second approach is to widen the bandwidth of the generator. This can be achieved by, for example, employing

- an array of structures each with a different resonant frequency;
- an amplitude limiter;
- coupled oscillators;
- non-linear (e.g. magnetic) springs;
- bi-stable structures;
- a large inertial mass (large device size) with a high degree of damping.

Details of these two types of adaptive kinetic energy harvesters will be studied and compared in the following three sections.

1.5 Strategies to Tune Resonant Frequency

1.5.1 Evaluating Tuning Approaches

Selection of tuning approaches will depend upon the application but in general some key factors for evaluating a tuning mechanism for adjusting the resonant frequency of kinetic energy harvesters are as follows:

- The energy consumed by the tuning mechanism should be as small as possible and must not exceed the energy produced by the generator.
- The mechanism should achieve a sufficient operational frequency range.
- The tuning mechanism should achieve a suitable degree of frequency resolution.
- The generator should have as high as possible Q-factor to achieve maximum power output and the strategy applied should not increase the damping, i.e. decrease Q-factor, over the entire operational frequency range.

Resonant frequency can be tuned by both mechanical and electrical methods. Mechanical tuning alters the resonant frequency by changing mechanical properties of the structure. Electrical tuning alters the resonant frequency by adjusting the electrical load. The principles of both methods and existing approaches to realize them are described in the following sections.

1.5.2 Mechanical Tuning Methods

As most reported vibration energy harvesting devices are based on a cantilever [2], focus will be on this structure in following theoretical analyses of mechanical tuning. Principles demonstrated are, however, generally applicable to all mechanical resonator structures. Tuning mechanisms covered in this section are

- changing dimensions;
- moving the centre of gravity of proof mass;
- variable spring stiffness;
- straining the structure.

After a brief analysis of the theory, a comprehensive review of each mechanical tuning mechanism reported in the literature to date is presented.

The resonant frequency of a spring-mass structure is given by

$$f_{\mathrm{r}} = \frac{1}{2\pi}\sqrt{\frac{k}{m}} \tag{1.46}$$

where k is the spring constant and m is the inertial mass. When tuning the resonant frequency of the generator, either the spring constant or the mass can be varied.

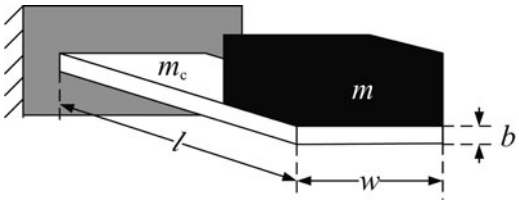

Fig. 1.11 Cantilever with a tip mass

The spring constant of a resonator depends on its materials and dimensions. For a cantilever with a mass at the free end (Fig. 1.11), the resonant frequency is given by [51]

$$f_r = \frac{1}{2\pi}\sqrt{\frac{Ywh^3}{4l^3(m + 0.24m_c)}} \tag{1.47}$$

where Y is Young's modulus of the cantilever material, w, h and l are the width, thickness and length of the cantilever, respectively, and m_c is the mass of the cantilever. The resonant frequency can be tuned by adjusting any of these parameters. In addition, it is important to mention that if actuators are involved in changing the mechanical properties of the resonant structure, the tuning mechanisms can be operated by a control system to automatically tune the generator. However, the energy cost of the actuator must be considered.

1.5.2.1 Changing Dimensions

It is difficult to change the width, w, and thickness, h, of a cantilever after it is made while changing its effective length, l, is feasible. The approach requires that the cantilever base clamp be released and re-clamped in a new location along the length of the beam thereby changing the effective length (and hence frequency). There is no power required to maintain the new resonant frequency. It is a method of intermittent tuning. Furthermore, as the resonant frequency is inversely proportional to $l^{3/2}$, modifying l can significantly change f_r.

Suppose l is the original length of the cantilever and l' is the modified length of the cantilever, $l' = l + \Delta$, where Δ is the difference between them. The mass of the cantilever is then changed to $m'_c = whl'\rho$, where ρ is the density of the cantilever material while the original mass of cantilever is $m_c = whl\rho$. Then, the new resonant frequency becomes

$$f'_r = \frac{1}{2\pi}\sqrt{\frac{Ywh^3}{4l'^3(m + 0.24m'_c)}} = \frac{1}{2\pi}\sqrt{\frac{Ywh^3}{4(l+\Delta)^3\{m + 0.24[wh(l+\Delta)]\rho\}}} \tag{1.48}$$

And the ratio of the tuned frequency to the original frequency called the normalized resonant frequency is

$$\frac{f_{\mathrm{r}}'}{f_{\mathrm{r}}} = \sqrt{\frac{l^3(m + 0.24m_{\mathrm{c}})}{l'^3(m + 0.24m_{\mathrm{c}}')}} = \sqrt{\frac{l^3(m + 0.24whl\rho)}{(l + \Delta)^3\{m + 0.24[wh(l + \Delta)]\rho\}}} \tag{1.49}$$

Figure 1.12 shows the normalized resonant frequency with the variation of cantilever length where a negative Δ/l means the new cantilever beam is shorter than its original length and thus has a higher resonant frequency. A positive Δ/l means the cantilever beam has been lengthened giving a lower resonant frequency. Figure 1.12 shows it is more efficient to tune the resonant frequency by shortening the cantilever beam.

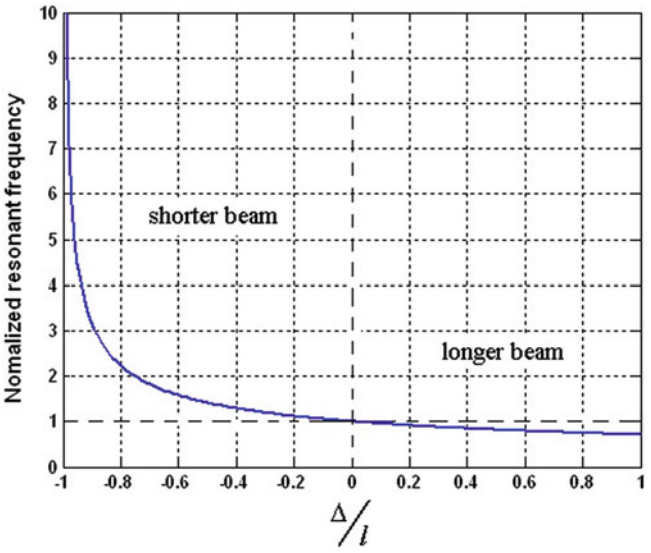

Fig. 1.12 Normalized resonant frequency with variation of cantilever lengths

An example of this approach is described in a patent by Gieras et al. [52]. Figure 1.13 shows the side view of the proposed device. The electromagnetic generator consists of a cantilever with a set of magnets fixed to its free end. The cantilever is clamped to a base using screws. A coil is placed between the magnets to pick up output power. A slider is connected to a linear actuator which moves the slider back and forth to adjust the effective length of the cantilever, L, and hence the resonant frequency of the generator.

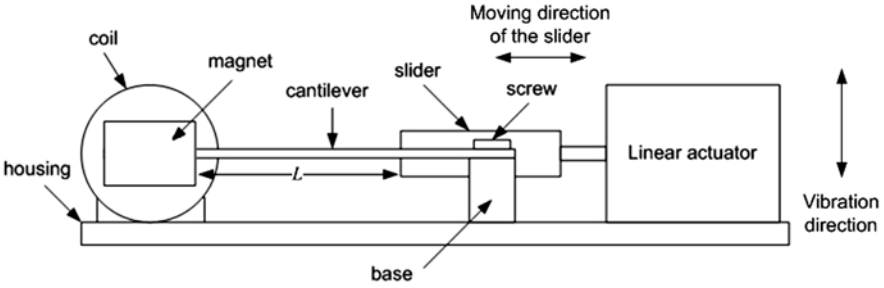

Fig. 1.13 Side view of a self-adjustable energy-harvesting system with variable effective lengths

1.5.2.2 Moving Centre of Gravity of Proof Mass

Once a generator has been fabricated, it is difficult to subsequently add or remove mass. However, the resonant frequency of a cantilever structure can be adjusted by moving the centre of gravity of the inertial mass. Figure 1.14 shows the side view of a cantilever with a mass on the free end.

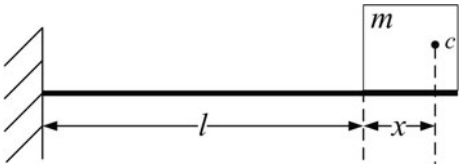

Fig. 1.14 Side view of a cantilever-mass structure

The length of the cantilever without the mass is l and the proof mass on its free end is m. The centre of gravity of the proof mass is located at c and the distance between c and the end of the cantilever is x. The tuned resonant frequency of this structure can be approximated as [53] (Fig. 1.15)

$$f_{\mathrm{r}}' = \frac{1}{2\pi}\sqrt{\frac{Ywh^3}{12ml^3}\cdot\frac{r^2+6r+2}{8r^4+14r^3+\frac{21}{2}r^2+4r+\frac{2}{3}}} \tag{1.50}$$

where w and h are the width and thickness of the cantilever, respectively, and $r = x/l$.

The resonant frequency of a cantilever-based generator, considering that the mass of the cantilever beam is negligible compared to the proof mass, Eq. (1.47), can be rewritten as

$$f_{\mathrm{r}} = \frac{1}{2\pi}\sqrt{\frac{Ywh^3}{4l^3m}} \tag{1.51}$$

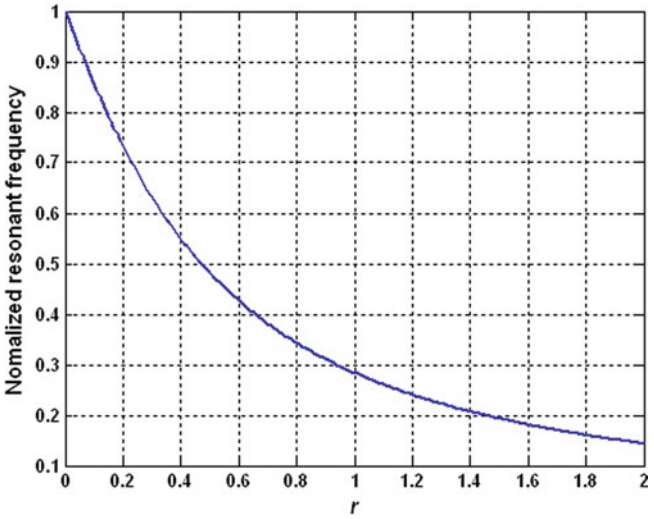

Fig. 1.15 Resonant frequency with variation of centre of gravity positions

Hence, the ratio of the tuned frequency to the original frequency is

$$\frac{f_{\mathrm{r}}'}{f_{\mathrm{r}}} = \sqrt{\frac{1}{3} \cdot \frac{r^2 + 6r + 2}{8r^4 + 14r^3 + \frac{21}{2}r^2 + 4r + \frac{2}{3}}} \tag{1.52}$$

Figure 1.14 shows the normalized resonant frequency with variation of the position of the centre of gravity of the proof mass. The closer the centre of gravity of the proof mass is from the end of the cantilever, the higher the resonant frequency.

Wu et al. [54] reported a piezoelectric generator using this principle as shown in Fig. 1.16. The proof mass of this device consists of a fixed mass and a movable mass. The position of the centre of gravity of the proof mass could be adjusted by changing the position of the movable mass. A fastening stud was used to fix the movable mass when tuning was finished. The size of the fixed mass is 10 mm × 12 mm × 38 mm and the movable mass is an M6 screw of length of 30 mm. The resonant frequency of the device was tuned from 180 to 130 Hz by moving the screw from one end to the other end (Fig. 1.17). The output voltage dropped with increasing resonant frequency. This approach is suitable for fine frequency tuning of the generator before installation and the vibration frequency in the working environment is not time varying. If the vibration frequency changes during operation, an actuator has to be employed on the cantilever to change the position of the movable mass, which increases the complexity of the generator.

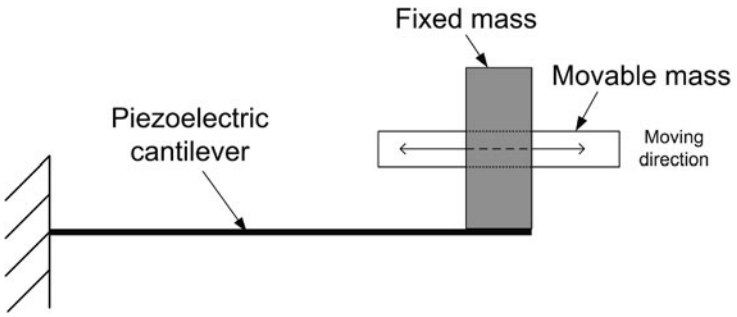

Fig. 1.16 A piezoelectric cantilever with movable mass

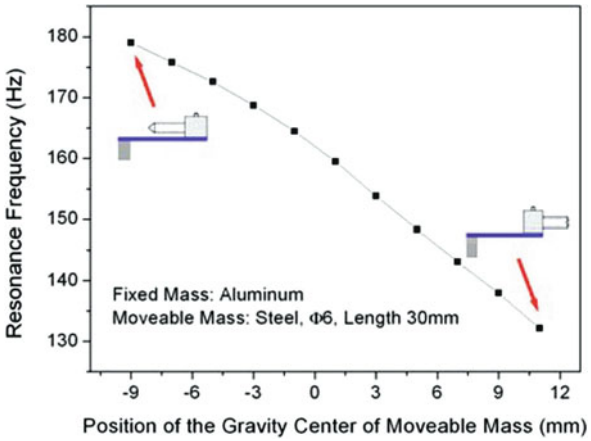

Fig. 1.17 Experimental result of frequency adjustment [54]

1.5.2.3 Variable Effective Spring Stiffness

Another commonly used method to tune the resonant frequency is to soften the spring stiffness. The principle is to apply a "negative" spring in parallel to the mechanical spring. Therefore, the effective spring constant of such device, k_{eff}, becomes

$$k_{\text{eff}} = k_{\text{m}} + k_{\text{a}} \tag{1.53}$$

where k_{m} is the mechanical spring constant and k_{a} is an additional "negative" spring stiffness as shown in Fig. 1.18. The modified frequency becomes

$$f_{\text{r}} = \frac{1}{2\pi}\sqrt{\frac{k_{\text{eff}}}{m}} = \frac{1}{2\pi}\sqrt{\frac{k_{\text{m}} + k_{\text{a}}}{m}} \tag{1.54}$$

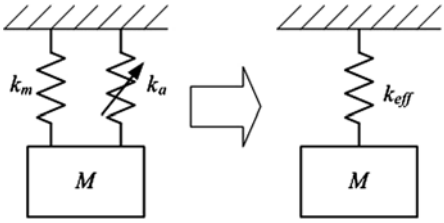

Fig. 1.18 Model of devices with softened spring stiffness

The negative spring k_a can be applied electrostatically, piezoelectrically, magnetically or thermally. Examples of these approaches are described below. Most of these examples are tunable resonators and not energy harvesters but the principles are identical. It is important to note, however, that the additional inertial mass present in an energy harvester (as opposed to the purely resonant structures) will reduce the tuning effectiveness and increase the power required to tune compared to the values quoted. It should also be noted that the following variable spring stiffness devices are all continuously operated except the one on which the negative spring is applied magnetically.

Electrostatic Methods

Scheibner et al. [55, 56] reported a vibration detector consisting of an array of eight comb resonators each with a different base resonant frequency. A single resonator is shown in Fig. 1.19. Each resonator comb is tuned by electrostatically softening the structure by applying a tuning voltage to the electrodes marked "V_{Tun}". The device was designed so that the resonator array had overlapping tuning ranges which allowed continuous measurements in the frequency range of the device from 1 to 10 kHz. Figure 1.20 shows the tuning range of each resonator. The tuning voltage varied from 0 to 35 V. The total size of the sensor chip is 7 mm $\times$ 10 mm.

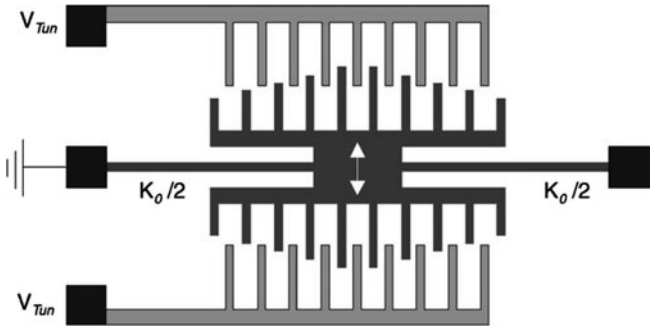

Fig. 1.19 Resonance tuning by electrostatic softening [56]

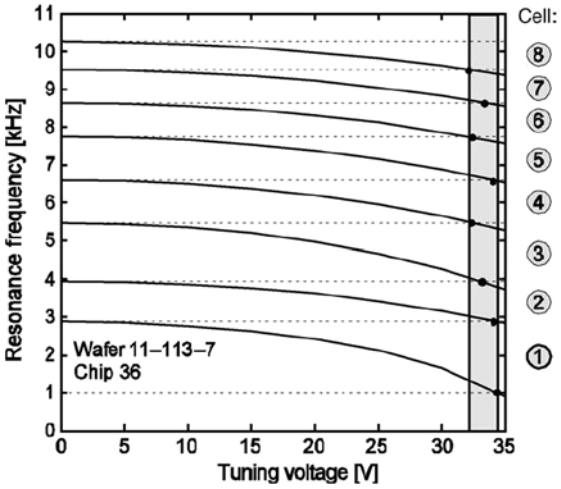

Fig. 1.20 Experimental results of the resonance tuning of the array [56]

Adams et al. [57] realized a tuning range from 7.7 to 146% of the central frequency of 25 kHz of a resonator with a single comb structure (Fig. 1.21). Figure 1.22 shows the tuning ranges of two of their devices under the driving voltage between 0 and 50 V. The total size was not mentioned in the chapter but is estimated from the SEM scale to be no larger than 500 μm $\times$ 500 μm.

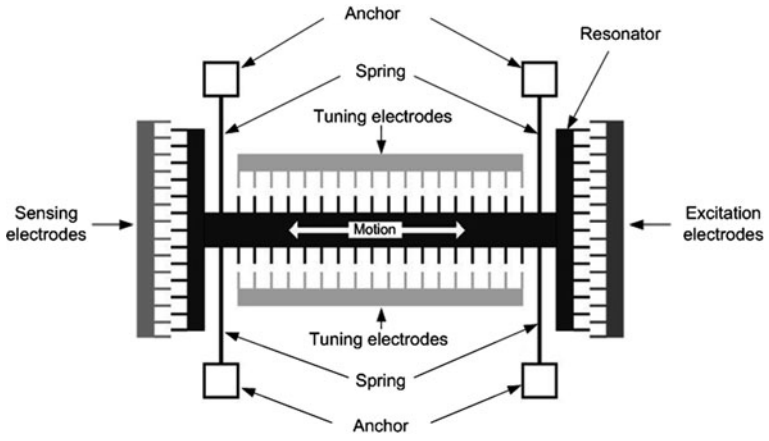

Fig. 1.21 Schematic diagram of single comb structure (after [57])

Lee et al. [58] presented a frequency-tunable comb resonator with curved comb fingers (Fig. 1.23). Fingers of the tuning comb were designed to be curved shape to generate a constant electrostatic stiffness or linear electrostatic force that is independent of the displacement of the resonator under a control voltage. Experimentally, the resonant frequency of a laterally driven comb resonator with 186 pairs of

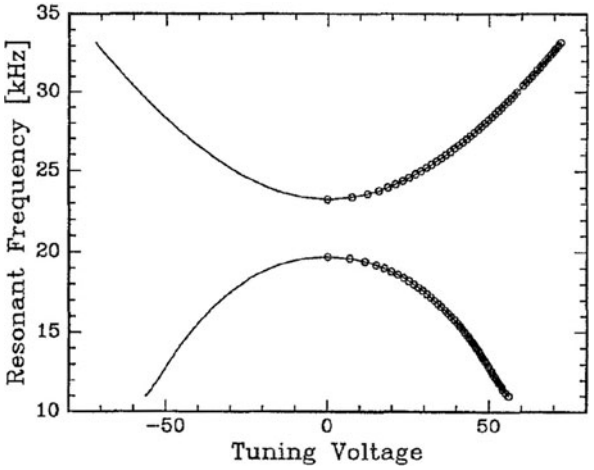

Fig. 1.22 Experimental results of resonance tuning of single comb structure [57]

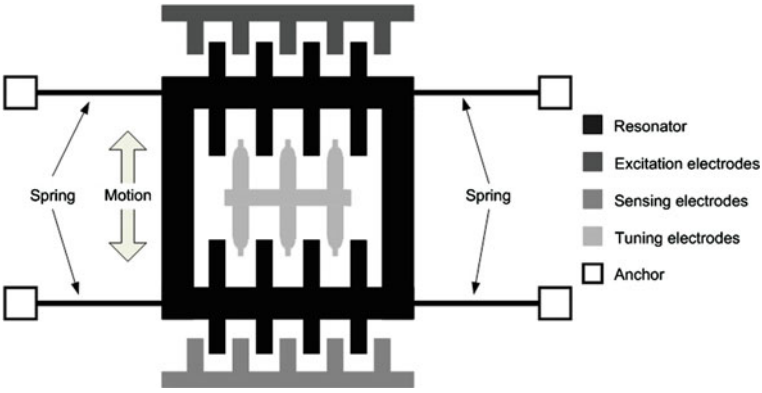

Fig. 1.23 Schematic diagram of comb resonator with curved tuning fingers (after [58])

curved contour fingers was reduced by 55% from the initial frequency of 19 kHz under a bias voltage of 150 V (Fig. 1.24). The corresponding effective stiffness was decreased by 80% from the initial value of 2.64 N/m. The total size of the resonator is 460 μm × 840 μm. It was concluded that the closed-form approach of the comb-finger profile can be applied to other comb-shaped actuators for frequency control while achieving linear electrostatic stiffness with respect to displacement.

Piazza et al. [59] developed a micromachined, piezoelectrically actuated and sensed, high-Q single-crystal silicon (SCS) resonator with voltage-tunable centre frequency (Fig. 1.25). Piezoelectric transduction was integrated with capacitive fine-tuning of the resonator centre frequency to compensate for any process variations. The resonant frequency could be tuned by 6 kHz based on an untuned resonant frequency of 719 kHz by applying an electrostatic force beneath the cantilever

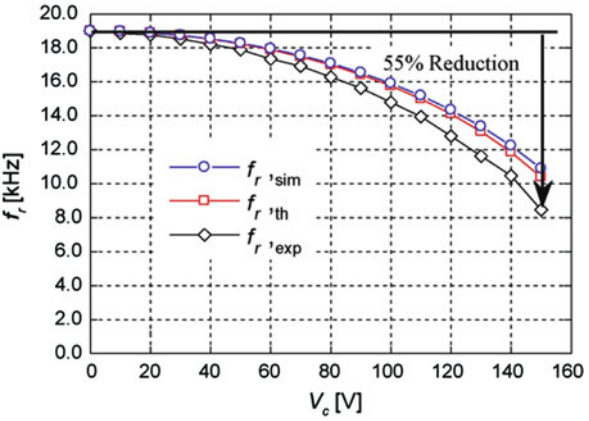

Fig. 1.24 Experimental results of resonance tuning of comb resonator with curved tuning fingers [58]

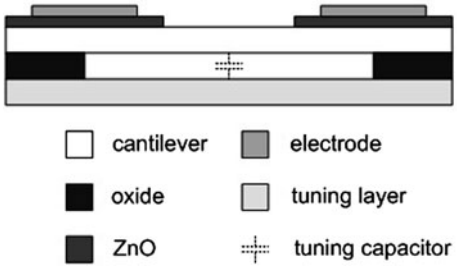

Fig. 1.25 Voltage-tunable, piezoelectrically transduced SCS resonators: Q-enhanced configuration (after [59])

(Fig. 1.26). The driving voltage varied from 0 to 20 V. The dimensions of this resonator are 200 μm × 20 μm × 4.2 μm.

Yao and MacDonald [60] compared frequency tuning by applying either axial force or transverse force on the resonator electrostatically as shown in Fig. 1.27. Frequency tuning by applying transverse force was tested experimentally. It was found that the resonant frequency may increase or decrease with the applied tuning voltage depending on where the tuning electrode is placed with respect to the excitation electrode and the resonating rod. When the tuning electrode was placed on the same side of the excitation electrode as indicated in Fig. 1.27b, the resonant frequency decreased with the increase of applied voltage. When the tuning electrode was placed on the opposite side of the excitation electrode as indicated in Fig. 1.27c, the resonant frequency increased with the increase of applied voltage.

A micromachined resonator having an out-of-plane natural resonant frequency of 149.5 kHz was tuned to 139.5 kHz by applying a DC tuning voltage of 30 V as shown in Fig. 1.28. The actual dimensions of these devices were not mentioned. Similar idea was later patented by Thiesen and O'Brian [61].

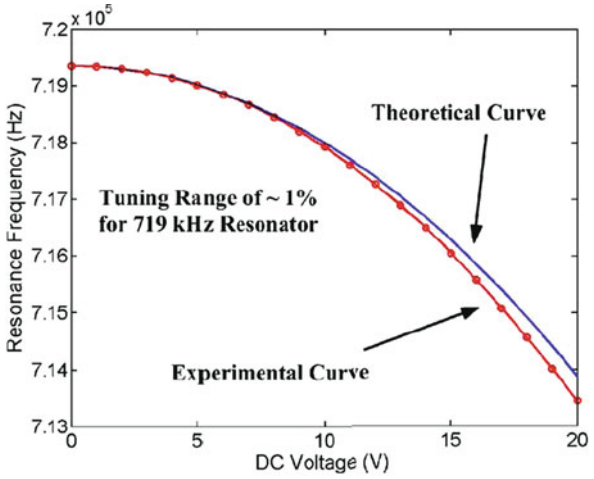

Fig. 1.26 Experimental results of resonance tuning of electrostatic fine-tuning characteristic for a 719 kHz piezo-resonator [59]

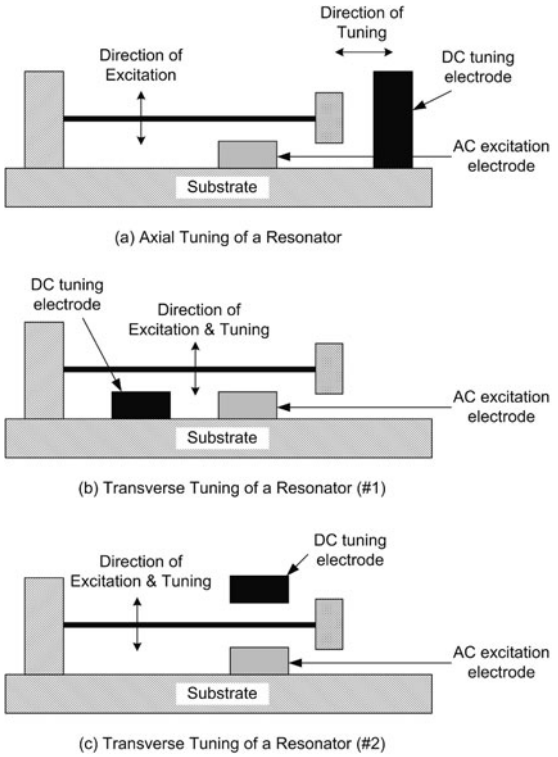

Fig. 1.27 Schematic drawing of a simple resonator showing axial loading (**a**), and transverse loading with the excitation and the tuning electrode on the same side (**b**) and on the opposite side (**c**) of the resonating rod [60]

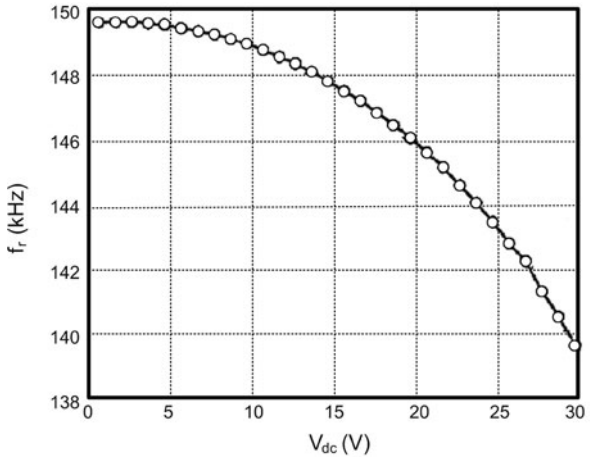

Fig. 1.28 Measured resonant frequency versus the tuning DC voltage with an untuned resonant frequency of 149.5 kHz (tuning mechanism as in Fig. 1.27b) [60]

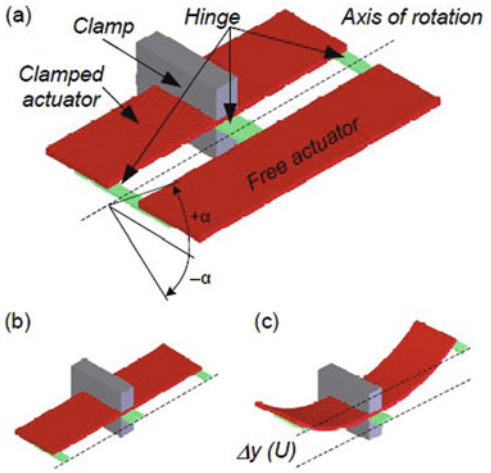

Fig. 1.29 (**a**) Schematic of the resonator (**b**) cross-section without applied voltage and (**c**) with applied voltage [62]

Piezoelectric Methods

Peters et al. [62] reported a tunable resonator, shown in Fig. 1.29a, potentially suitable as a resonator structure for vibration energy harvesting. The resonant frequency is tuned by mechanically stiffening the structure using piezoelectric actuators. A piezoelectric actuator was used because piezoelectric materials can generate large forces with low power consumption. Two actuators, one clamped and one free, are connected together. The free actuator can oscillate around the axis

of rotation if a suitable excitation is applied to the clamp. The stiffness of the structure was increased by applying an electrical potential to both actuators which changes the shape of the structure as shown in Fig. 1.29c. Thus, the natural frequency of the rotational mass-spring system increased. The tuning voltage was chosen to be ±5 V leading to a measured resonance shift of ±15% around the initial resonant frequency of 78 Hz, i.e. the tuning range was from 66 to 89 Hz (Fig. 1.30).

Wischke et al. [63] presented an electromagnetic vibration scavenger that exhibits a tunable resonant frequency as shown in Fig. 1.31. The resonant frequency can be tuned by applying a static electrical field on the piezoelectric cantilever. This feature is originated from exploiting the elastostriction of the utilized piezoelectric bimorph suspension. It is demonstrated that the resonant frequency has been tuned from 267 to 323 Hz when a tuning voltage between −100 and 260 V is applied.

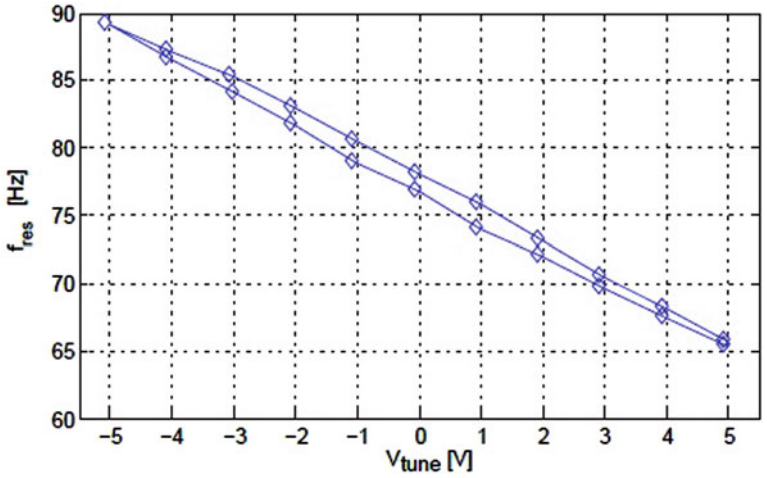

Fig. 1.30 Measured resonant frequency versus applied tuning voltage [62]

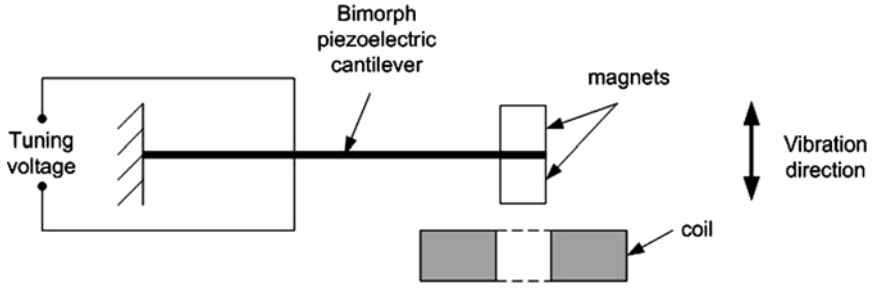

Fig. 1.31 A piezoelectrically tunable electromagnetic generator (after [63])

Magnetic Methods

Challa et al. [64] reported an intermittently tuned piezoelectric micro-generator (Fig. 1.32), 50 cm^3 in volume, with a frequency range of 22–32 Hz based on an original resonant frequency of 26 Hz. The tuning was realized by applying a magnetic force perpendicular to the cantilever generator as shown in Fig. 1.33. The resonant frequency of the generator can be tuned by changing the distance between the two sets of tuning magnets and the fixed magnets. The maximum tuning distance was 3 cm. Experimentally, the generator produced 240–280 μW power at 0.8 m s^{-2} acceleration. However, the tuning mechanism had the unwanted side effect of varying damping over the frequency range as shown in Fig. 1.33. The device was made of discrete components. The dimension of the piezoelectric cantilever is 34 mm × 20 mm × 0.92 mm and the effective mass is 45.8 g.

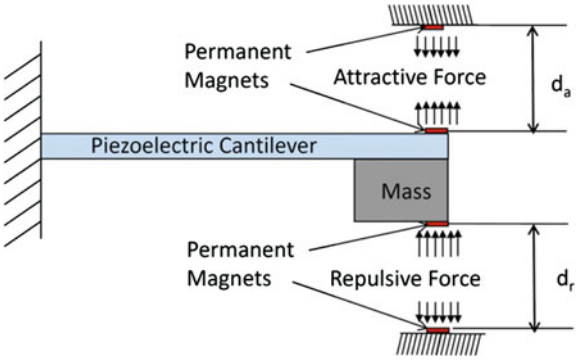

Fig. 1.32 Schematic of the tunable piezoelectric generator [64]

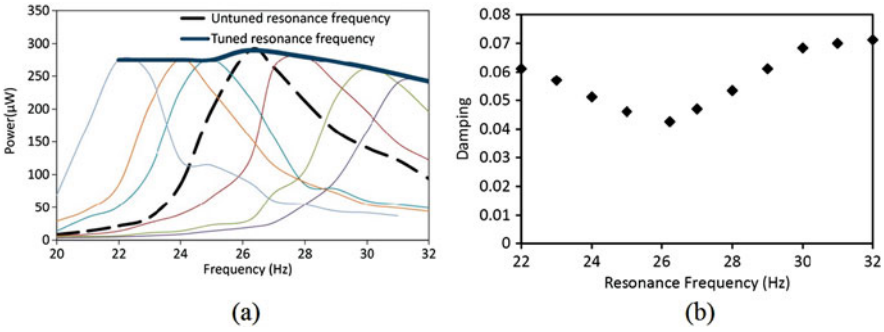

Fig. 1.33 Output power (**a**) and damping (**b**) versus resonant frequency [64]

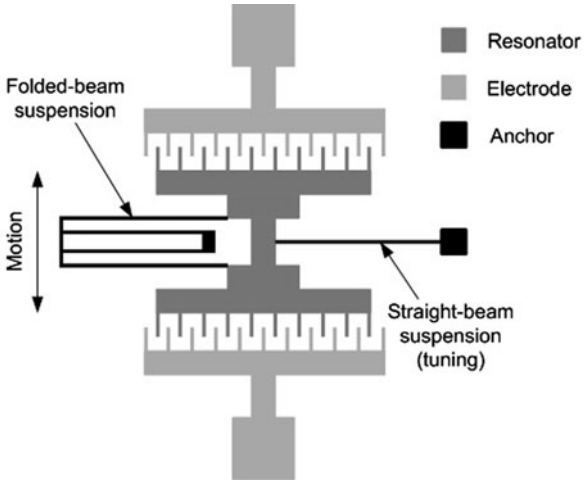

Fig. 1.34 Schematic diagram of a comb-shaped micro-resonator with a straight-beam for active frequency tuning via localized stressing effects (after [65])

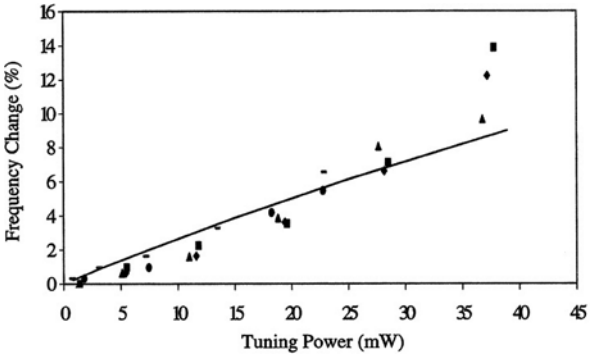

Fig. 1.35 Measured frequency change versus tuning power [65]

Thermal Methods

Remtema and Lin [65] applied a thermal stress on a straight-beam spring using a resistive heater (Fig. 1.34), which resulted in a maximum 6.5% frequency change based on a resonant frequency of 31 kHz with a maximum temperature at 255°C. The power consumption during the process was 25 mW. Figure 1.35 shows the percentage change of resonant frequency with variation of power consumed in tuning. The size of the device is estimated to be less than 500 μm $\times$ 700 μm from the authors' description.

Syms [66] reported frequency tuning by applying constrained thermal expansion on a simple unfolded resonator (Fig. 1.36). The tuning range was from -25 to $+50\%$ with power consumption from 1.5 to 10 mW (Fig. 1.37). The tuning sen-

sitivity obtained with this tuning method was 33% mW^{-1}. It is estimated from the annotation in Fig. 1.36 that the device is no larger than 3000 μm × 3000 μm.

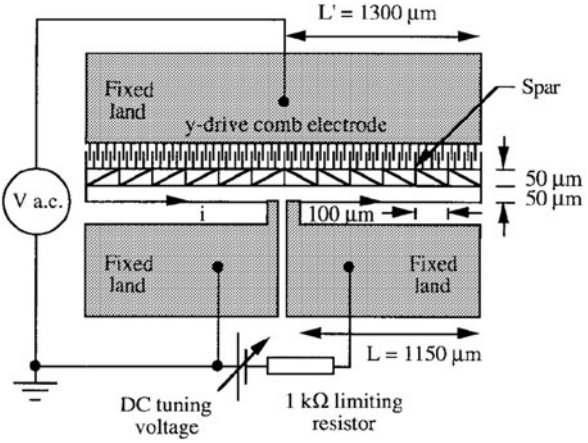

Fig. 1.36 Layout and connection of laterally resonant comb-drive actuator used for tuning experiments [66]

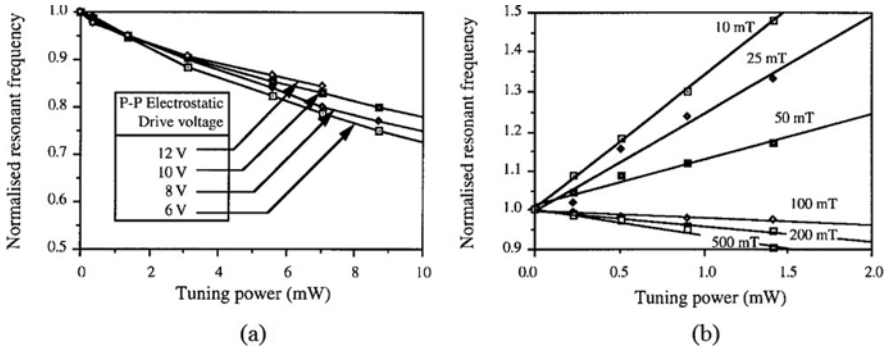

Fig. 1.37 Variation of resonant frequency with tuning power (**a**) at different electrostatic drive voltages and (**b**) gas pressures [66]

The thermal approach is unlikely to be practical for energy harvesting since it consumes too much power compared to the power generated by a kinetic energy harvester and is a continuous tuning mechanism.

1.5.2.4 Straining the Structure

The effective stiffness of the structure can be varied by applying a stress and therefore placing it under strain. The following theoretical analyses focus on straining a cantilever and a double-clamped beam. The resonant frequency of both these structures can be tuned by applying an axial load. In vibration energy harvesting,

most devices are based on beam structures, especially the cantilever (Fig. 1.38). An axial tensile load applied to a beam (Figs. 1.38a and 1.39a) increases the resonant frequency while an axial compressive load (Figs. 1.38b and 1.39b) decreases the resonant frequency of the beam.

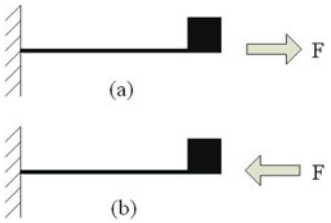

Fig. 1.38 Axial tensile (**a**) and compressive (**b**) loads on a cantilever

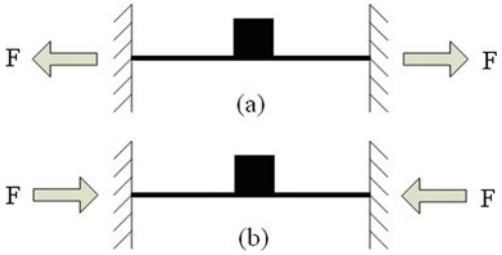

Fig. 1.39 Axial tensile (**a**) and compressive (**b**) loads on a double-clamped beam

An approximate formula for the resonant frequency of a uniform cantilever in mode i with an axial load, f_{ri}, is given by [51]

$$f'_{\mathrm{r}i} = f_{\mathrm{r}i} \cdot \sqrt{1 + \frac{F}{F_{\mathrm{b}}} \cdot \frac{\lambda_1^2}{\lambda_i^2}} \tag{1.55}$$

where f_{r} is the resonant frequency in mode i without load, F is the axial load and F_{b} is the axial load required to buckle the beam, i.e. to cause the fundamental resonant frequency zero. F is positive for a tensile load and negative in the compressive case. Variable λ_i is a dimensionless load parameter which is a function of the beam boundary conditions applied to the cantilever for the ith mode of the beam. It is given by the ith positive solution of Eq. (1.56) for a cantilever and of Eq. (1.57) for a double-clamped beam [51].

$$\cos\lambda \cdot \cosh\lambda + 1 = 0 \tag{1.56}$$

$$\cos\lambda \cdot \cosh\lambda - 1 = 0 \tag{1.57}$$

The majority of cantilever-based energy harvesters operate in the fundamental flexural mode (mode 1); the resonant frequency of a uniform cantilever in mode 1

with an axial load, f_{r1}, is given by

$$f'_{r1} = f_{r1} \cdot \sqrt{1 + \frac{F}{F_b}} \tag{1.58}$$

The ratio of the tuned frequency to the original frequency is

$$\frac{f'_{r1}}{f_{r1}} = \sqrt{1 + \frac{F}{F_b}} \tag{1.59}$$

The buckling load F_b of a cantilever and a clamped–clamped beam are given by Eqs. (1.60) and (1.61), respectively [60]:

$$F_{b\_can} = \frac{\pi^2 Y w h^3}{48 l^2} \tag{1.60}$$

$$F_{b\_dcb} = \frac{\pi^2 Y w h^3}{3 l^2} \tag{1.61}$$

where Y is Young's modulus of the material of the cantilever and w, h and l are the width, thickness and length of the cantilever, respectively.

Figure 1.40 shows the change in resonant frequency of a cantilever with an applied axial load. It shows that a compressive load is more efficient in frequency tuning than a tensile load. If the compressive force is larger than the buckling load, the cantilever beam will buckle and no longer oscillate in mode 1. If a very large

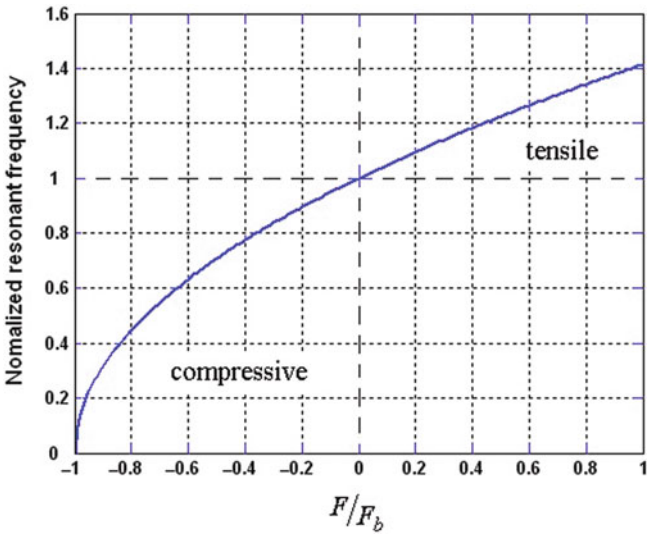

Fig. 1.40 Normalized resonant frequency with variation of axial loads

tensile force is axially applied to the cantilever, i.e. much greater than the buckling load, the resonant frequency will approach that of a straight-tensioned cable as the force associated with the tension in the cantilever becomes much greater than the beam stiffness.

Double-Clamped Beam Structures

Cabuz et al. [67] realized resonant frequency tuning by an applying axial force on a micromachined resonant beam electrostatically as shown in Fig. 1.41. One end of the resonator was clamped on a fixed support while the other end was connected to a movable support. The movable support could rotate around a torsion bar as a voltage was applied across two tuning electrodes. The torsion bar converted the vertical tuning motion into an axial force along the resonator. Upward rotation induces a compressive stress in the resonator while downward rotation induces a tensile stress. The tuning range was 16 Hz based on a centre frequency of 518 Hz (Fig. 1.42) with driving voltage from 0 to 16 V. The dimensions of the resonator are 1000 μm × 200 μm × 3 μm and the dimensions of the movable support are 12.5 mm^2 × 0.3 mm. This is an example of continuous tuning.

Leland and Wright [68] successfully tuned the resonant frequency of a vibration-based piezoelectric generator by applying an axial compressive preload directly on the cantilever (Fig. 1.43). The tuning range was from 200 to 250 Hz. Experimentally, the generator produced an output power between 300 and 400 μW at an acceleration of 9.8 m s^{-2}. It was determined that a compressive axial preload could reduce the resonance frequency of a vibration energy scavenger by up to 24% but it also increased the total damping (Fig. 1.44). The piezoelectric bimorph has

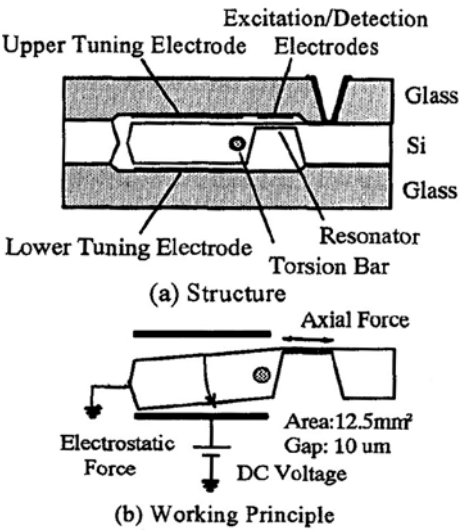

Fig. 1.41 Structure for fine resonance frequency tuning at device level by an electrostatically induced axial force [67]

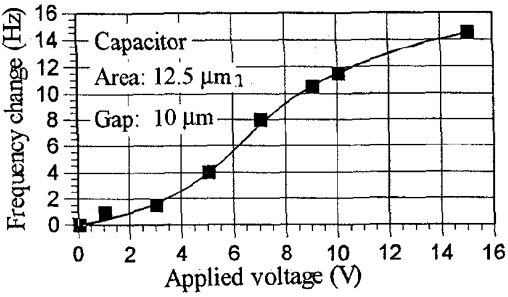

Fig. 1.42 Resonant frequency change versus applied voltage [67]

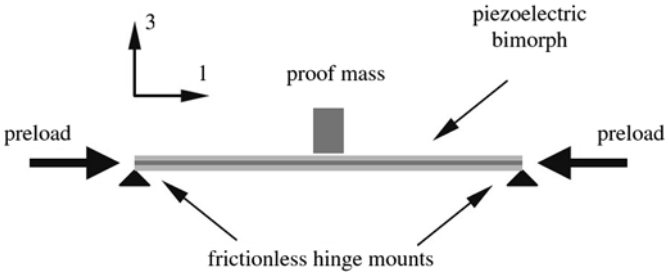

Fig. 1.43 Schematic of a simply supported piezoelectric bimorph vibration energy scavenger [68]

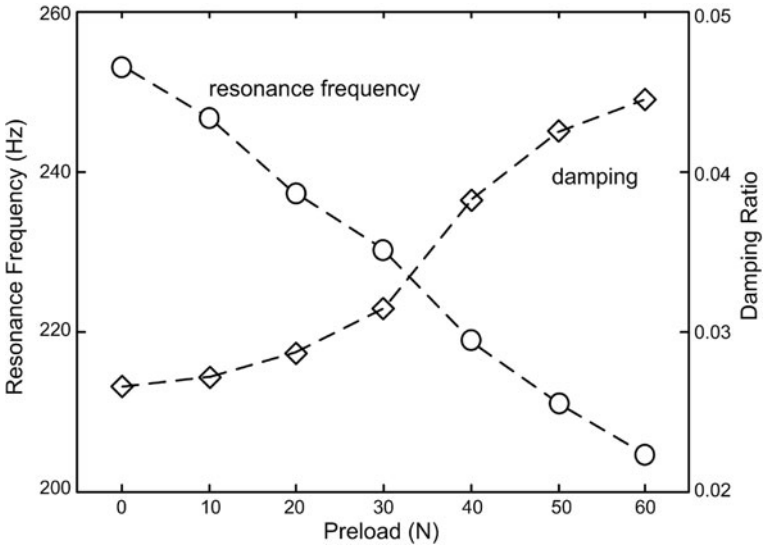

Fig. 1.44 Resonance frequency and damping versus preload [68]

dimensions of 31.7 mm × 12.7 mm × 0.509 mm and the weight of the proof mass is 7.1 g. This is an example of intermittent tuning, but it is not automated and has to be done manually.

Cantilever Structures

Mukherjee [69] patented the idea of applying axial force to a vibrating cantilever beam sensing element using electrostatic force. The resonator consisted of two sets of comb-like structures (Fig. 1.45). The set closer to the anchor was used for sensing while the other set was used for frequency tuning. A voltage was applied between the two fixed tuning electrodes and the structure at the free end to apply an axial tensile or compressive end load to the cantilever. The resonant frequency of the beam was approximately 15.5 kHz. This is an example of continuous tuning which achieved a tuning range of −0.6 to 3.3% of its untuned resonant frequency, i.e. about 600 Hz. The cantilever buckled when 50 V_{DC} was applied to provide a compressive force. This is an example of continuous tuning.

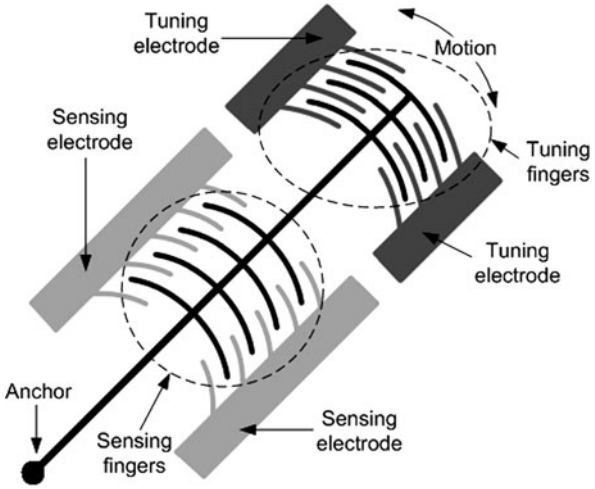

Fig. 1.45 Resonator with actuator at the free end

Hu et al. [70] theoretically investigated an axial preloading technique to adjust the behaviour of a piezoelectric bimorph. It was found analytically that this mechanism can improve the performance of the piezoelectric bimorph at varying frequency vibrations. A method for applying an axial preload to a piezoelectric bimorph was suggested and is shown in Fig. 1.46. It comprises a mechanical bolt running through the central metal layer and fixed at the left-hand side edge wall. A capped stiff metal plate was attached to the bolt at the free end of the cantilever. A clockwise torsion of the bolt can produce a compressive preload to the bimorph and, conversely, an anticlockwise torsion of the bolt produces a force to pull the capping plate towards the right-hand side, which can generate a tensile preload to the bimorph. This is an example of manual intermittent tuning.

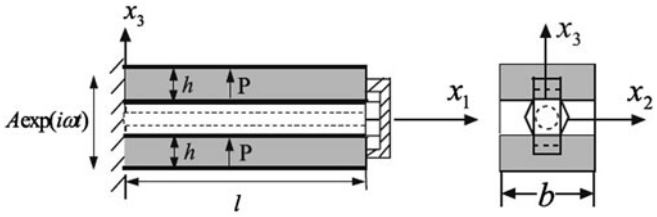

Fig. 1.46 A method to apply axial preload to a piezoelectric bimorph [70]

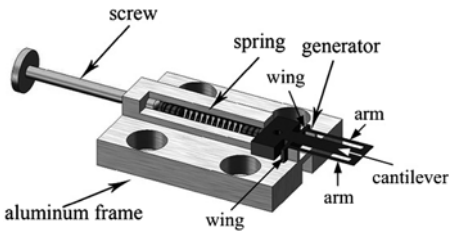

Fig. 1.47 Schematic diagram of the test device [71]

This principle was demonstrated by Eichhorn et al. [71]. Figure 1.47 shows a schematic diagram of the test device. The piezoelectric generator consisted of a piezo-polymer-composite cantilever beam with arms on both sides to enable the application of an axial force to the free end of the beam. The arms were connected to the base with two wings. These wings were used to transmit the force to the arms, which in turn apply the load to the free end of the beam. The tuning force was applied by a screw and a steel spring. The axial load depends linearly on the deflection of the spring, which in turn was proportional to the number of revolutions of the screw. The spring pushes the whole generator base against two blocks of which the counter-pressure generates the pre-stress in the arms and the stabilizing wings. The screw, spring and generator were all mounted on the same aluminium frame. This is another example of manual intermittent tuning.

In tests only a compressive load was applied. Figure 1.48 shows the test results of this generator under vibration level of 63.7 m s^{-2}. It was found that with the increase of compressive load, the resonant frequency, output voltage and the Q-factor reduced. By cutting notches on the wings the tuning efficiency could be increased. With notches in the wings, a resonant frequency shift of more than 20% was achieved with a total force of 22.75 N (Fig. 1.49). The tuning range was from 290 to 380 Hz with compressive load up to 22.75 N. The dimensions of the cantilever are 20 mm × 5 mm × 0.44 mm and the overall width of the device including arms is 13 mm.

A non-contact method of applying axial load to a cantilever-based micro-generator is reported by Zhu et al. [72, 73] who presented a tunable electromagnetic vibration-based micro-generator with closed-loop frequency tuning. Frequency tuning was realized by applying an axial tensile magnetic force to the micro-generator (Fig. 1.50).

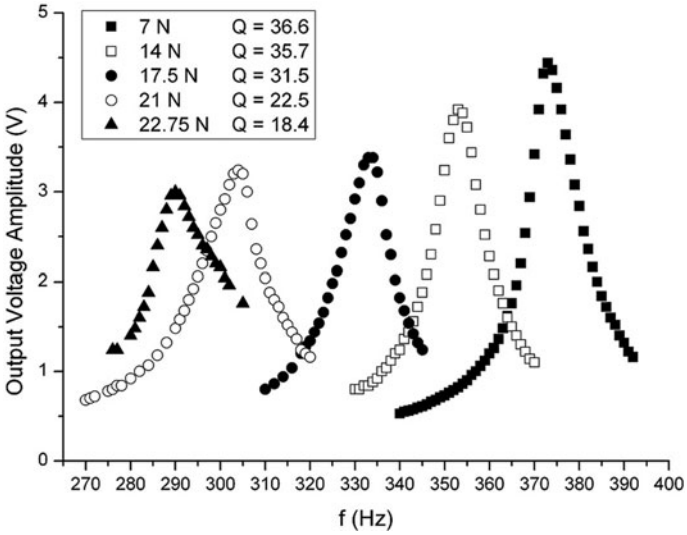

Fig. 1.48 Test results under vibration of 63.7 m s^{-2} [71]

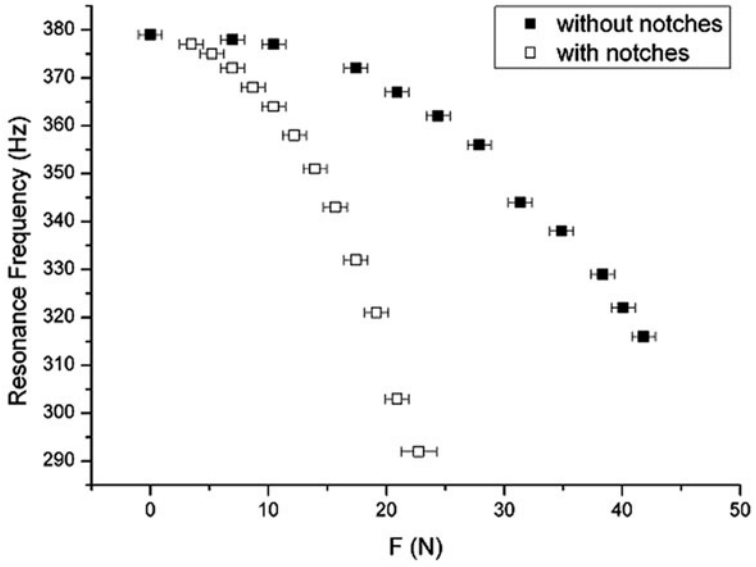

Fig. 1.49 Comparison of tuning efficiency of wings with and without notches [71]

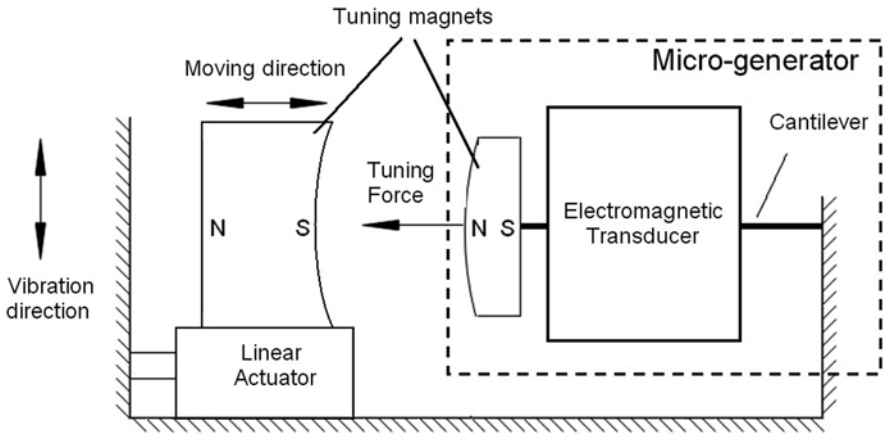

Fig. 1.50 Schematic diagram of the tuning mechanism [72]

The tuning force was provided by the attractive force between two tuning magnets with opposite poles facing each other. One magnet was fixed at the free end of a cantilever while the other was attached to an actuator and placed axially in line with the cantilever. The distance between the two tuning magnets was adjusted by the linear actuator. Thus, the axial load on the cantilever and hence the resonant frequency was changed. The areas where the two magnets face each other were curved to maintain a constant gap between them over the amplitude range of the generator. Figure 1.51 shows the test results of the resonant frequency variation of distance between the two tuning magnets. The tuning range of the proposed micro-generator was from 67.6 to 98 Hz based on the original resonant frequency of 45 Hz by changing the distance between two tuning magnets from 5 to 1.2 mm.

Experimentally, the generator produced a power of 61.6–156.6 μW over the tuning range when it was excited at a constant vibration acceleration level of 0.59 m s^{-2}. It was also found that the tuning mechanism does not affect the damping of the micro-generator over 60% of the tuning range. However, when the tuning force becomes larger than the inertial force caused by vibration, total damping is increased and the output power is less than expected from theory (see resonant peaks at 92 and 98 Hz in Fig. 1.52).

1.5.3 Electrical Tuning Methods

All the frequency tuning methods mentioned above are based on mechanical methods. In this section, methods to tune the resonant frequency of a vibration-based micro-generator electrically will be detailed.

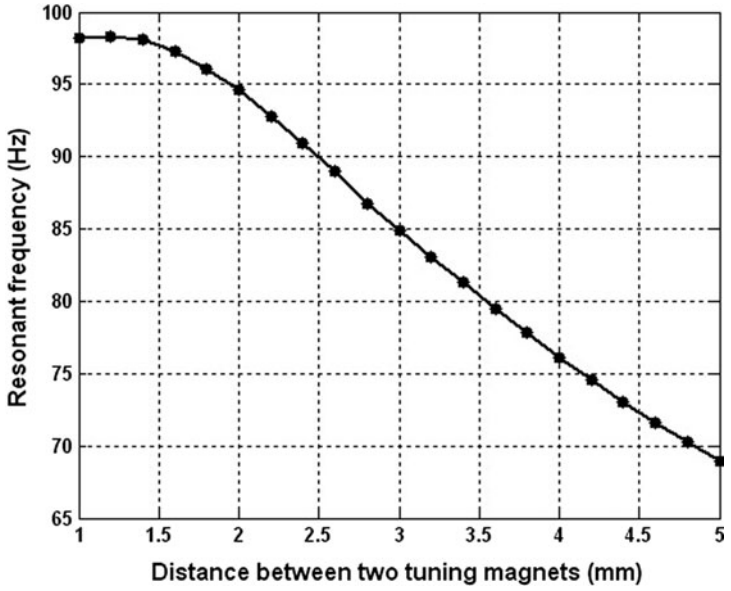

Fig. 1.51 Resonant frequency with variance of distances between two tuning magnets [72]

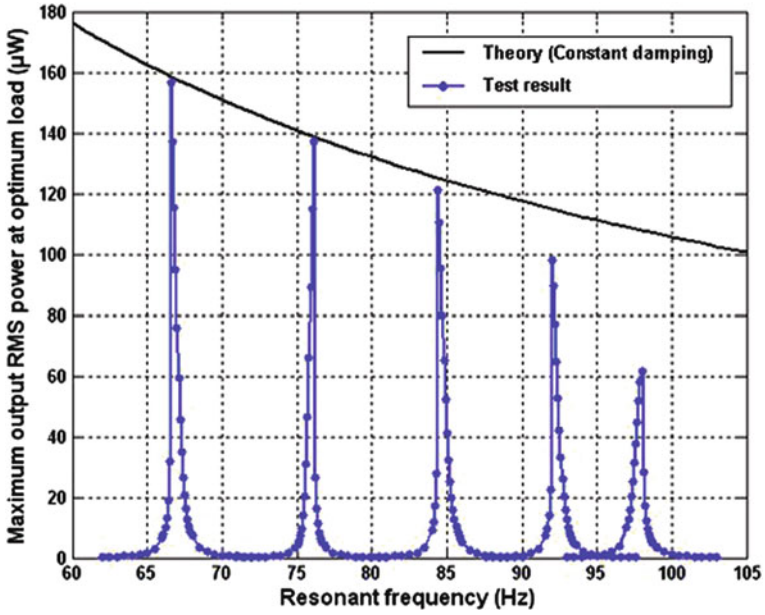

Fig. 1.52 Power spectrum of the micro-generator (excited at 0.59 m s^{-2}) [72]

1.5.3.1 Principles

The basic principle of electrical tuning is to change the electrical damping by adjusting the electrical load. As all reported generators using electrical tuning are piezoelectric, in this section, only the piezoelectric micro-generator will be addressed. As resistive loads reduce the efficiency of power transfer and load inductances are difficult to be varied, it is most feasible to adjust capacitive loads to realize electrical tuning.

Figure 1.53 shows a schematic diagram of a bimorph piezoelectric generator with a mass, m, on the tip. l_b and l_m are the effective length of the cantilever and mass, respectively. w is the width of the cantilever. t_p and t_s are the thickness of the piezoelectric layer and substrate layer, respectively, and t_g is the distance from the centre of the substrate layer to the centre of the piezoelectric layer. Electrodes of the generator have been omitted in Fig. 1.53.

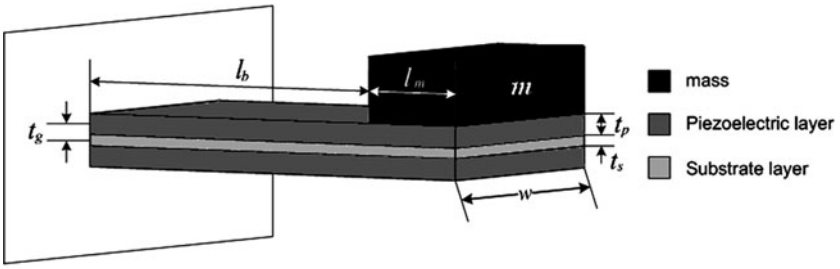

Fig. 1.53 Piezoelectric bimorph generator

This bimorph piezoelectric generator can be represented using an equivalent circuit as shown in Fig. 1.54. L_m, R_m and C_m represent the mass, damping, and spring in the mechanical part, respectively. C_p is the capacitance of the piezoelectric layer, C_L and R_L are the capacitive and resistive loads, respectively. V is the RMS voltage across the resistive load.

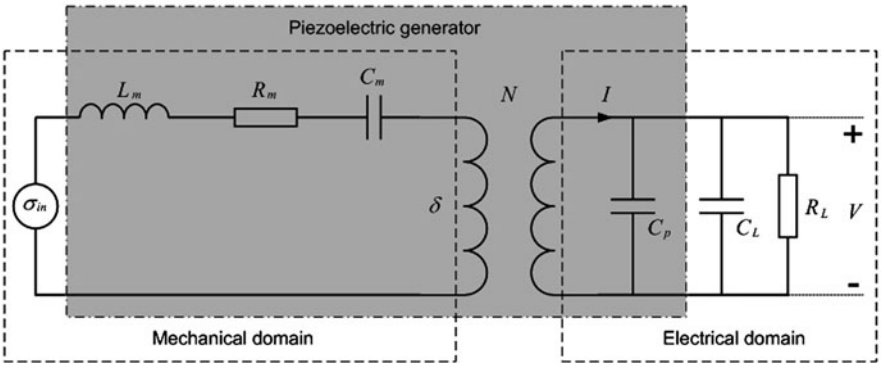

Fig. 1.54 Equivalent circuit of piezoelectric generator with capacitive and resistive loads

The transformer relates the mechanical domain to the electrical domain according to the model of the piezoelectric effect. Specifically, it relates stress (σ) to electric field (E) at zero strain or electrical displacement (D) to strain (δ) at zero electric field. Rewriting equations for piezoelectric effect, which have been described in Eqs. (1.31) and (1.32), leads to the equations for the transformer as

$$D = -d_{31} Y_{\mathrm{p}} \delta \tag{1.62}$$

where d_{31} is the piezoelectric strain coefficient in 31 mode and Y_{p} is Young's modulus of the piezoelectric material.

Hence, the transform ratio N is given by

$$N = -d_{31} Y_{\mathrm{p}} \tag{1.63}$$

Equation (1.64) can be derived to present the mechanical dynamics of the system with electrical coupling. Detailed derivation of this model can be found in [21].

$$\Delta(s^2 + 2\zeta\omega_{\mathrm{r}} s + \omega^2) = \frac{\omega_{\mathrm{r}}^2 d_{31} a}{2t_{\mathrm{c}}} V + b^* A_{\mathrm{in}} \tag{1.64}$$

where Δ is Laplace transform of strain, δ, A_{in} is the vibration acceleration, ζ is the damping factor, ω_{r} is the untuned resonant frequency, $a = 1$ if the two piezoelectric layers are connected in series and $a = 2$ if they are connected in parallel and s is the Laplace variable. b^* is given by

$$b^* = \frac{3t_{\mathrm{g}}}{l_{\mathrm{b}}^2} \cdot \frac{2l_{\mathrm{b}} + l_{\mathrm{m}} - l_{\mathrm{e}}}{2l_{\mathrm{b}} + \frac{3}{2} l_{\mathrm{m}}} \tag{1.65}$$

where l_{e} is the length of the electrodes.

Furthermore, analysis in the electrical domain gives the following equation:

$$\Delta = \left(s + \frac{1}{R_{\mathrm{L}} C_{\mathrm{pL}}}\right) \frac{V C_{\mathrm{pL}}}{s\Sigma} \tag{1.66}$$

where $C_{\mathrm{pL}} = C_{\mathrm{p}} + C_{\mathrm{L}}$ and $\Sigma = -a \cdot d_{31} \cdot Y_{\mathrm{c}} \cdot l_{\mathrm{e}} \cdot w$. l_{e} is the length of the electrodes.

Combining Eqs. (1.64) and (1.66) gives the transfer function of the system as

$$\frac{V}{A_{\mathrm{in}}} = \frac{s\Sigma b^*}{s^3 + \left(\frac{1}{R_{\mathrm{L}} C_{\mathrm{pL}} + 2\zeta\omega_{\mathrm{r}}}\right) s^2 + \left(\omega_{\mathrm{r}}^2 + \frac{2\zeta\omega_{\mathrm{r}}}{R_{\mathrm{L}} C_{\mathrm{pL}}} - \frac{a\Sigma\omega_{\mathrm{r}}^2 d_{31}}{2t_{\mathrm{c}}}\right) s + \frac{\omega_{\mathrm{r}}^2}{R_{\mathrm{L}} C_{\mathrm{pL}}}} \tag{1.67}$$

which leads to the expression of the voltage across the resistive load given by

$$V(\omega) = \frac{j\omega \Sigma b^* A_{\text{in}}}{\left[\frac{\omega_{\text{r}}^2}{R_{\text{L}}} - \left(\frac{1}{R_{\text{L}}} + 2\zeta\omega_{\text{r}} C_{\text{pL}}\right)\omega^2\right] + j\omega\left[(\omega_{\text{r}}^2 - \omega^2)C_{\text{pL}} + \frac{2\zeta\omega_{\text{r}}}{R_{\text{L}}} - \frac{a\Sigma\omega_{\text{r}}^2 d_{31}}{2t_{\text{c}}}\right]} \tag{1.68}$$

The power in the resistive load is given by

$$\begin{aligned} P(\omega) &= \frac{V(\omega)^2}{R_{\text{L}}} \\ &= \frac{1}{R_{\text{L}}} \cdot \frac{(\omega \Sigma b^* A_{\text{in}})^2}{\left[\frac{\omega_{\text{r}}^2}{R_{\text{L}}} - \left(\frac{1}{R_{\text{L}}} + 2\zeta\omega_{\text{r}} C_{\text{pL}}\right)\omega^2\right]^2 + \omega^2\left[(\omega_{\text{r}}^2 - \omega^2)C_{\text{pL}} + \frac{2\zeta\omega_{\text{r}}}{R_{\text{L}}} - \frac{a\Sigma\omega_{\text{r}}^2 d_{31}}{2t_{\text{c}}}\right]^2} \end{aligned} \tag{1.69}$$

It is known that $f(x, y) = x^2 + y^2 \leq 2xy$ and that $f(x, y)$ becomes a minimum only if $x = y$ (i.e. $\frac{1}{f(x,y)}$ is maximum only if $x = y$). Therefore, Eq. (1.69) reaches maximum when

$$\frac{\omega_{\text{r}}^2}{R_{\text{L}}} - \left(\frac{1}{R_{\text{L}}} + 2\zeta\omega_{\text{r}} C_{\text{pL}}\right)\omega^2 = \omega\left[(\omega_{\text{r}}^2 - \omega^2)C_{\text{pL}} + \frac{2\zeta\omega_{\text{r}}}{R_{\text{L}}} - \frac{a\Sigma\omega_{\text{r}}^2 d_{31}}{2t_{\text{c}}}\right] \tag{1.70}$$

Rearranging Eq. (1.70) leads to a cubic function of the form

$$\omega^3 + X\omega^2 + Y\omega + Z = 0 \tag{1.71}$$

where

$$\begin{aligned} X &= -\left(\frac{1}{R_{\text{L}} C_{\text{pL}}} + 2\zeta\omega_{\text{r}}\right) \\ Y &= -\left(\omega_{\text{r}}^2 + \frac{2\zeta\omega_{\text{r}}}{R_{\text{L}} C_{\text{pL}}} - \frac{a\Sigma\omega_{\text{r}}^2 d_{31}}{2t_{\text{c}} C_{\text{pL}}}\right) \\ Z &= \frac{\omega_{\text{r}}^2}{R_{\text{L}} C_{\text{pL}}} \end{aligned}$$

The real solution of Eq. (1.71) gives the function of resonant frequency with respect to the load capacitance as

$$\omega(C_{\text{L}}) = \frac{\sqrt[3]{\Omega + 12\sqrt{\Psi}}}{6} - \frac{2(Y - \frac{X^2}{3})}{\sqrt[3]{\Omega + 12\sqrt{\Psi}}} - \frac{X}{3} \tag{1.72}$$

where $\Omega = 36XY - 108Z - 8X^3$ and $\Psi = 12Y^3 - 3X^2Y^2 - 54XYZ + 81Z^2 + 12X^3Z$.

Equations (1.69) and (1.72) indicate that output power and the resonant frequency of a bimorph piezoelectric generator vary with variations of the load capacitance. Figure 1.55 compares the resonant frequencies and power output of electrically tunable piezoelectric generators of different piezoelectric materials with

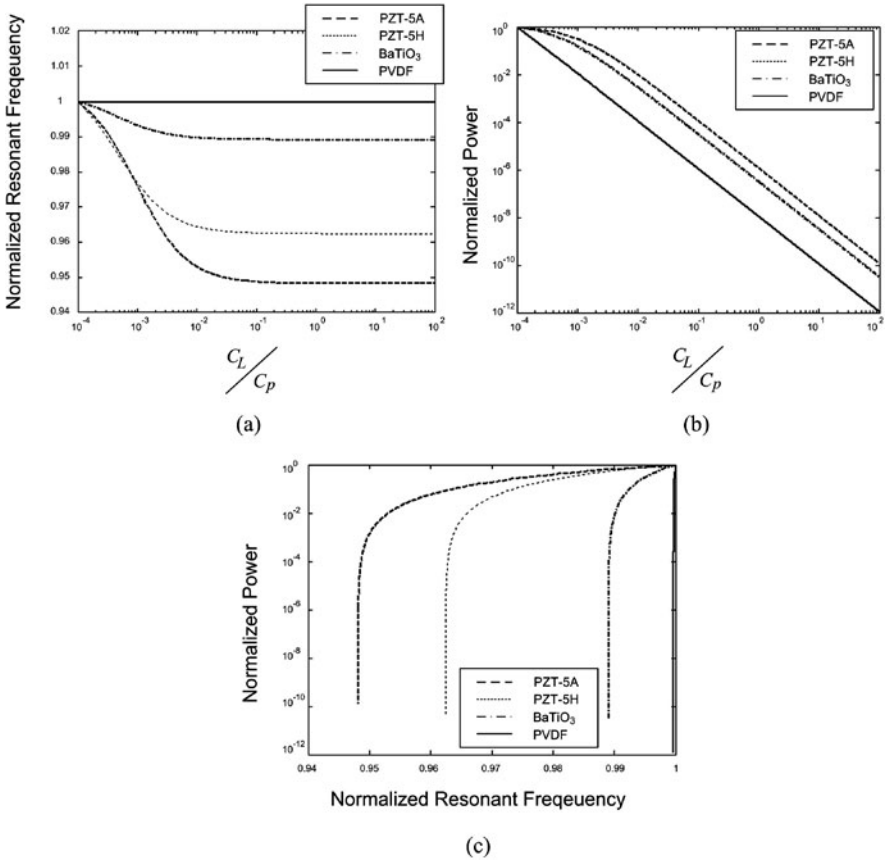

Fig. 1.55 Performance of a piezoelectric generator with different piezoelectric materials: (**a**) Resonant frequency (**b**) output power; and (**c**) output power versus resonant frequency

variation of load capacitances. These generators are identical except for the piezoelectric material. The coefficients used in the simulation are listed in Table 1.2.

The resonant frequency as well as the output power reduces with increasing load capacitance. It was found that PZT-5H is the best of these four piezoelectric materials for an electrically tunable piezoelectric generator. Important considerations relating to the tunability of the piezoelectric generator are as follows:

- The material of the substrate layer and mass does not affect the tunability.
- A piezoelectric material with higher Young's modulus, strain coefficient and smaller permittivity provides a larger tuning range.
- The ratio of the thickness of the piezoelectric layer to the thickness of the substrate layer should be small to increase the tuning range.
- The capacitance of the piezoelectric layer should be minimized to increase the tuning range.

- If both piezoelectric layers are used for tuning, connection of these two layers in parallel gives a larger tuning range than connection in series.
- The total damping should be kept low to increase the tuning range.

1.5.3.2 Examples of Electrically Tunable Micro-generators

Wu et al. [74] used this method to tune the resonant frequency of a generator composed of a piezoelectric bimorph cantilever. The upper piezoelectric layer was used for frequency tuning while the lower layer was used for energy harvesting. The tunable bandwidth of this generator was 3 Hz between 91.5 and 94.5 Hz. The charging time of the generator was compared with and without the tuning system. Experimentally, it was found that, when the device was excited under random frequencies from 80 to 115 Hz, the average harvesting output power of the generator with tuning was about 27.4% higher than that without tuning and the charging time was shortened by using tuning system. These results showed a significant improvement of average harvested power output by using an electrical tuning method.

Charnegie [75] presented another piezoelectric micro-generator based on a bimorph structure and adjusted its load capacitance. Again, one piezoelectric layer was designed for energy harvesting while the other is used for frequency tuning (Fig. 1.56).

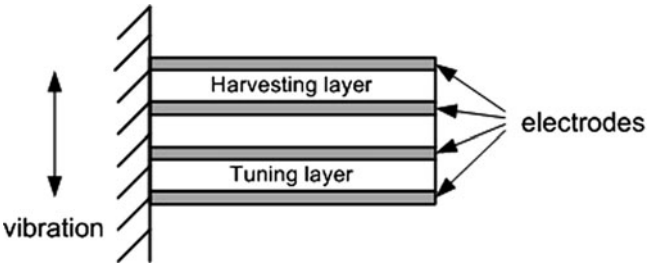

Fig. 1.56 Piezoelectric bimorph used for electrical frequency tuning

The test results showed that if only one layer was used for frequency tuning (Fig. 1.57a), the resonant frequency can be tuned an average of 4 Hz with respect to the untuned frequency of 350 Hz, i.e. 1.14% tuning by adjusting the load capacitance from 0 to 10 mF (Fig. 1.58a). If both layers were used for frequency tuning (Fig. 1.57b), the tuning range was an average of 6.5 Hz, i.e. 1.86% of tuning by adjusting the same amount of the load capacitance (Fig. 1.59a). It was found that if one layer was used for tuning and the other for energy harvesting (Fig. 1.57a), the output power did not reduce with the increase of the load capacitance (Fig. 1.58b). However, if both frequency tuning and energy harvesting were achieved using the same layer (Fig. 1.57b), the output power decreased when the load capacitance became larger (Fig. 1.59b).

Cammarano et al. [76] presented a vibration-based energy harvester whose resonant frequency can be tuned by varying its electrical load (containing both real

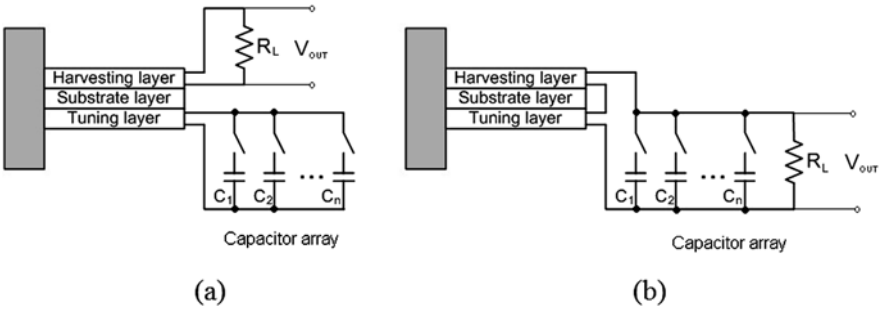

Fig. 1.57 Frequency tuning and energy harvesting using (**a**) the same layers and (**b**) different layers

and reactive impedances). It was found experimentally that the −3 dB (half-power) bandwidth of the energy harvester (16 Hz) is over three times greater when presented with an optimized load impedance compared to that for the same harvester presented with an optimized resistive-only load (4.5 Hz). They also developed an analytical model of the system. Readers may refer to their paper for more details if interested.

1.6 Strategies to Widen Bandwidth

The other commonly used solution to increase the operational frequency range of kinetic energy harvesters is to widen the bandwidth. To date, strategies to widen the bandwidth include using a generator array consisting of small generators with different resonant frequencies, introducing an amplitude limiter to the device, using coupled oscillators, employing non-linear and bi-stable structures and designing a large generator with a large inertial mass and high degree of damping. In this section, details of generator array, amplitude limiter and non-linear and bi-stable structures will be covered. The strategy of employing a single large generator will not be detailed as it can be simply described using Eq. (1.14) while it will be considered in the comparison of different strategies later in Section 1.7.

1.6.1 Generator Array

A generator array consists of multiple small generators, each of which has different dimensions and mass and hence different resonant frequencies (Fig. 1.60). Thus, the assembled generator has a wide operational frequency range while the Q-factor does not decrease. Figure 1.61 shows the power spectrum of a generator array which is a combination of the power spectra of each small generator. The operational frequency band of the generator is thus essentially increased. The drawback of this approach is the added complexity of fabricating an array of generators and the increased total volume of the device depending upon the number of devices in the array.

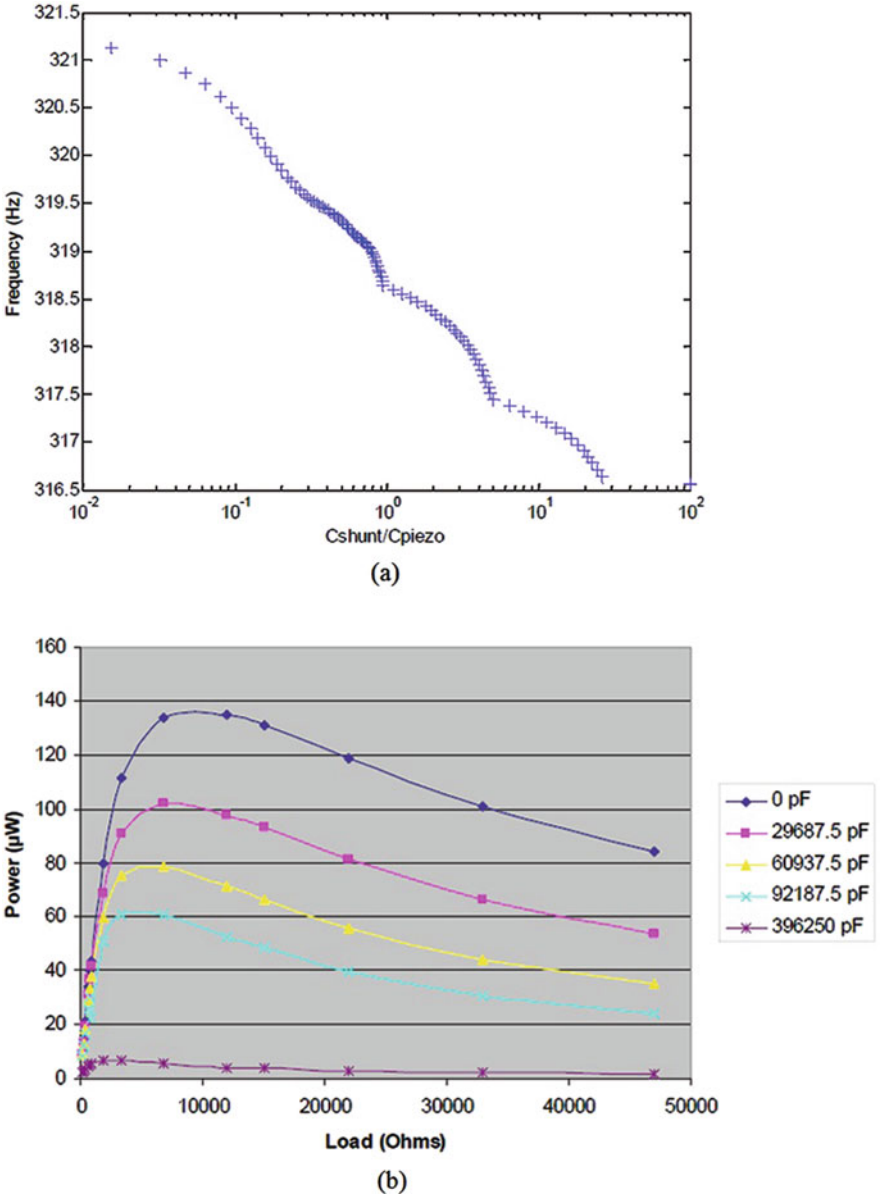

Fig. 1.58 (**a**) Resonant frequency and (**b**) output power versus load capacitance while tuning and energy harvesting in different layers [75]

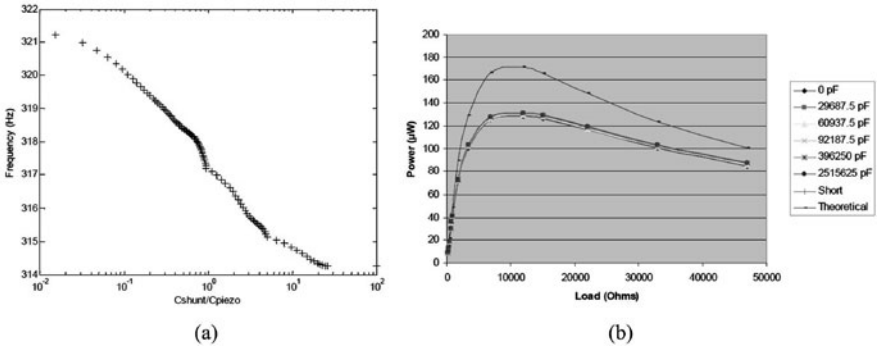

Fig. 1.59 (**a**) Resonant frequency and (**b**) output power versus load capacitance while tuning and energy harvesting in same layers [75]

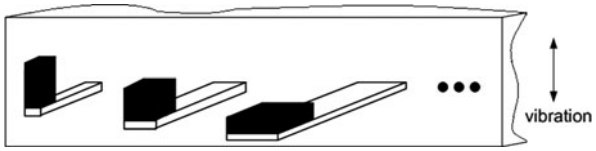

Fig. 1.60 A mechanical band-pass filter with a set of cantilever beams

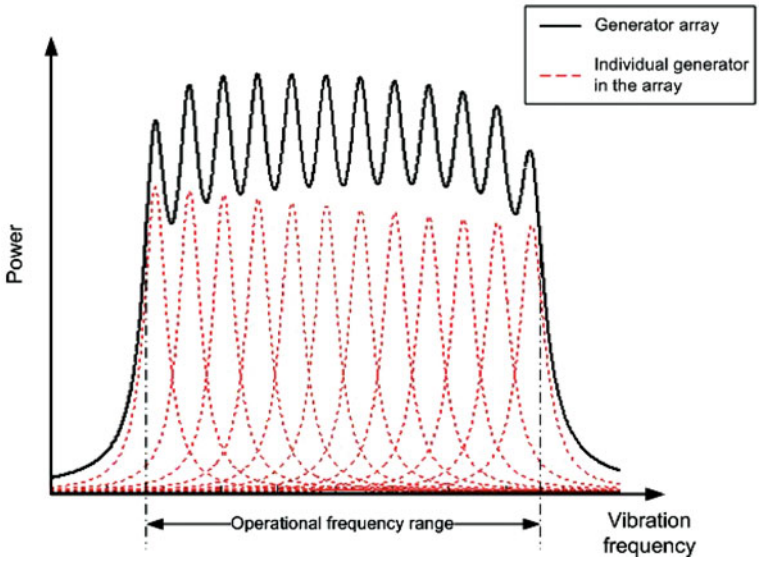

Fig. 1.61 Power spectrum of a generator array

Xue et al. [77] presented a broadband piezoelectric harvesters consisting of multiple piezoelectric bimorphs with different thicknesses of piezoelectric layers. It was found analytically that the bandwidth of a generator can be widened by connecting multiple piezoelectric bimorphs with different dimensions in series. In addition, the bandwidth of the generator can be shifted to the dominant frequency domain of the ambient vibrations by increasing or decreasing the number of piezoelectric bimorphs in parallel. Numerical results showed that the bandwidth of the piezoelectric energy harvesting devices can be tailored by the connection patterns (i.e. in series and in parallel) among piezoelectric bimorphs (Figs. 1.62 and 1.63).

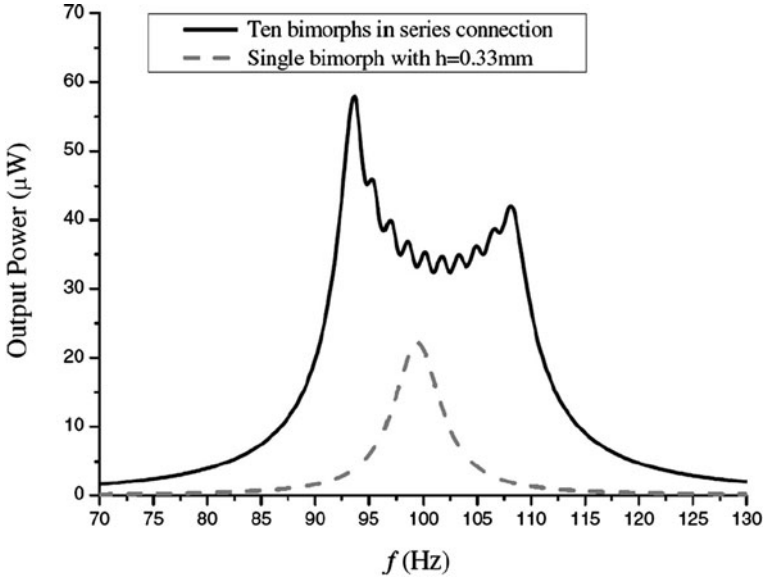

Fig. 1.62 Comparison of power spectrum for a single piezoelectric bimorph and 10 piezoelectric bimorphs in series with various thicknesses of piezoelectric layer [77]

Feng and Hung [78] presented a micromachined piezoelectric generator with a wide bandwidth. The device was designed to achieve an optimal figure of merit (FOM) which is defined as $(\text{bandwidth})^2 \times$ (the maximum displacement of cantilever structures under a given acceleration under static conditions). The generator consisted of four cantilever structures connected in parallel and has dimensions of 3 mm × 3 mm × 5 mm. These cantilevers had different masses or centre of gravity and hence different resonant frequencies (Fig. 1.64). The designed generator was targeted at producing microwatts to milliwatts in a wide mechanical vibration range from 300 to 800 Hz (Fig. 1.65) but no test results were reported to date.

A multifrequency piezoelectric generator intended for powering autonomous sensors from background vibrations was presented by Ferrari et al. [79]. The generator consisted of multiple bimorph cantilevers with different natural frequencies of which the rectified outputs were fed to a single storage capacitor. A generator

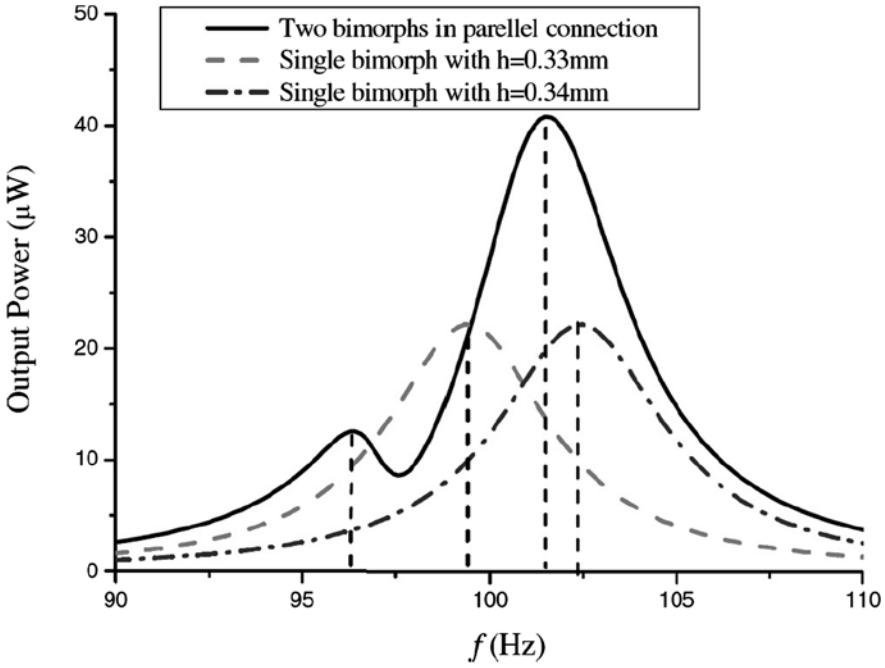

Fig. 1.63 Effect of piezoelectric bimorphs in parallel on harvester performance [77]

with three commercially available piezoelectric bimorph cantilevers was examined. Each cantilever has the same dimensions of 15 mm × 1.5 mm × 0.6 mm and different masses, 1.4, 0.7, and 0.6 g, respectively. The generator was used to power a battery-less sensor module. It was concluded that a generator array operating with wideband frequency vibrations provides improved overall energy conversion over a single generator at the expense of larger volume.

Sari et al. [80] reported a micromachined electromagnetic generator with a wide bandwidth. The generator consists of a series of cantilevers with various lengths and hence resonant frequencies (Fig. 1.66). These cantilevers are distributed in a 12.5 mm × 14 mm area. The length of the cantilevers increased gradually so that the cantilevers have overlapping frequency spectra with the peak powers at similar but different frequencies. This resulted in a widened bandwidth as well as an increase in the overall output power. Experimentally, the device generated 0.5 μW continuous power at 20 mV voltage between 3.3 and 3.6 kHz of ambient vibration. Figure 1.67 shows the power spectrum of this generator.

Lin et al. [81] reported a multi-cantilever piezoelectric MEMS generator, which has the ability to scavenge mechanical energy of ambient vibrations and transforms it into useful electrical power. The generator comprises four cantilever-type devices, two mode 31 devices and two mode 33 devices, which were made by a silicon process in a single die. The four cantilever devices can be connected in series or in parallel so as to possess different output characteristics. The measurement results

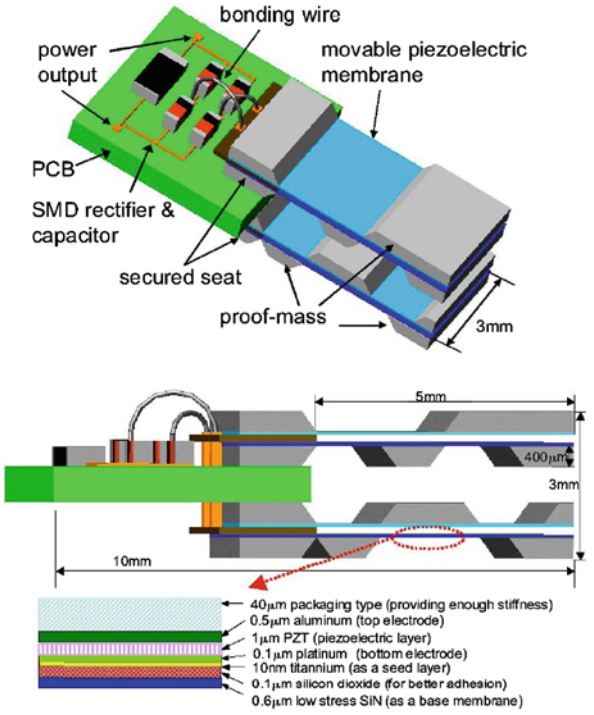

Fig. 1.64 Conceptual diagram of the piezoelectric wide bandwidth micro-generator [78]

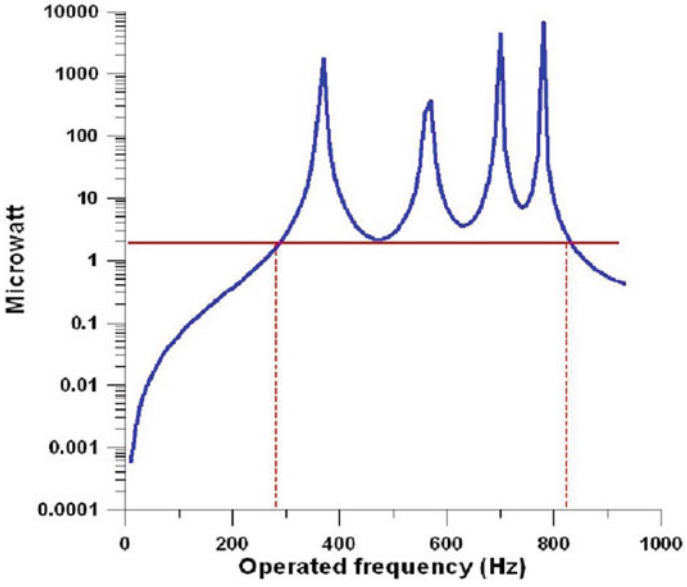

Fig. 1.65 Estimated power generation with the power range of microwatts to milliwatts in a wide bandwidth [78]

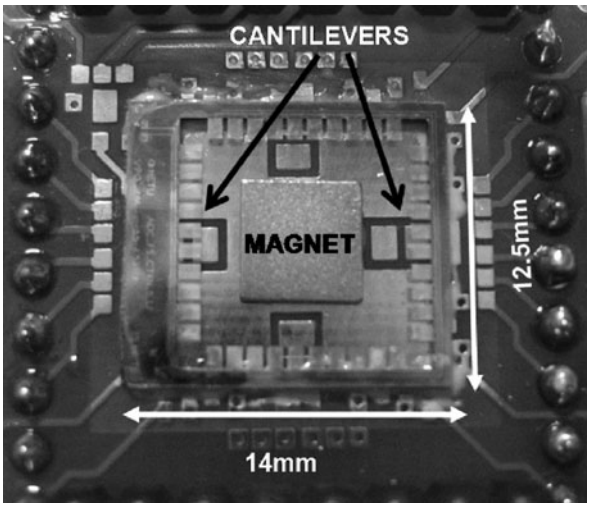

Fig. 1.66 Photograph of a wideband electromagnetic generator [80]

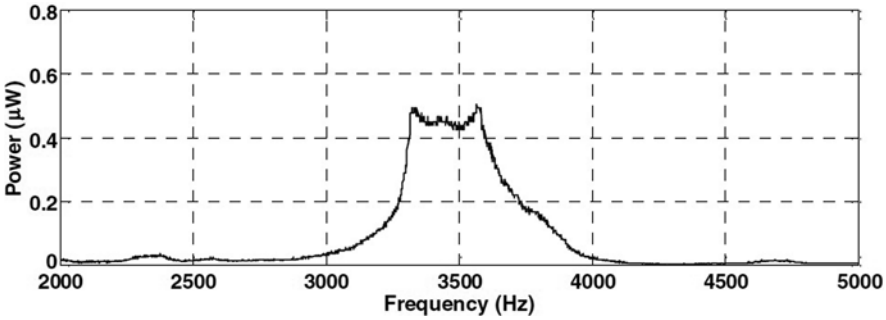

Fig. 1.67 Power spectrum of Sari's generator [80]

show that the prototype device possesses resonance frequencies between 237 and 244.5 Hz. However, no information of output power has been given.

1.6.2 Amplitude Limiter

Another method of increasing the bandwidth of a vibration-based micro-generator was reported by Soliman et al. [82, 83]. The bandwidth of the device was increased by using a mechanical stopper (amplitude limiter) to limit the amplitude of the resonator (Figs. 1.68 and 1.69). The theory behind this method is complex and details can be found in [82]. This method can increase the bandwidth of the generator when the excitation frequency was gradually increased. However, the bandwidth remained the same when excitation frequency was gradually reduced. Experimental measurements showed that the bandwidth was 240% wider than that of the archi-

tecture without a stopper at the half-power level but the maximum output voltage was 30% less (Fig. 1.70) in the case when the excitation frequency was increased. The dimensions of the cantilever are 45.3 mm × 10 mm × 1.02 mm and the mass is extrapolated to be 2.92 g. It should be noted that since this principle relies on continuous physical contact with the cantilever, it is unlikely to provide a reliable long-term solution for increasing bandwidth.

1.6.3 Coupled Oscillators

The method of widening the operational bandwidth of the MEMS generator using coupled oscillators was reported by Petropoulos et al. [84]. The proposed generator has a pair of coupled oscillators that consist of two springs, two masses and two dampers. The first spring connects the inertial frame and the first mass while the second spring connects the two mass while each mass has a damper to the frame as shown in Fig. 1.71. The analytic model shows that this type of generators has flat response for power generation over a wider frequency range. However, the maximum output power of the generator is significantly decreased than that of the generator with one mass (Fig. 1.72).

1.6.4 Non-linear Generators

The theory of vibration energy harvesting using non-linear generators was investigated by Ramlan et al. [85]. Instead of using conventional second-order model as Eq. (1.1), non-linear generators were modelled using Duffing's equation as follows:

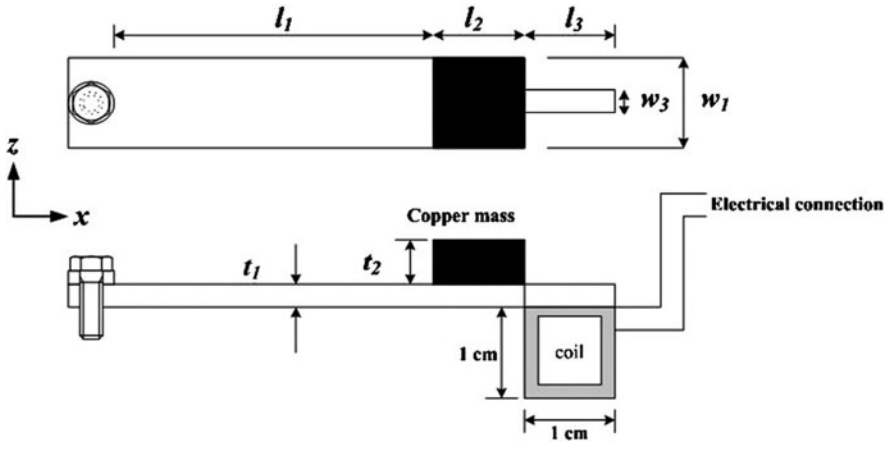

Fig. 1.68 *Top* and *side* views of the device [82]

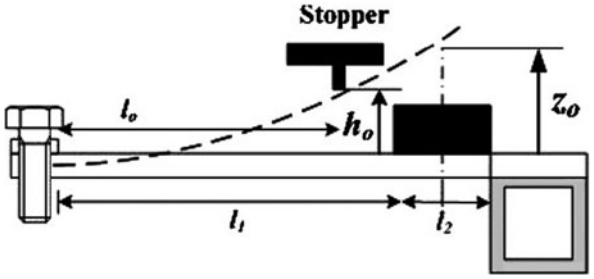

Fig. 1.69 Increase the bandwidth using an amplitude limiter [82]

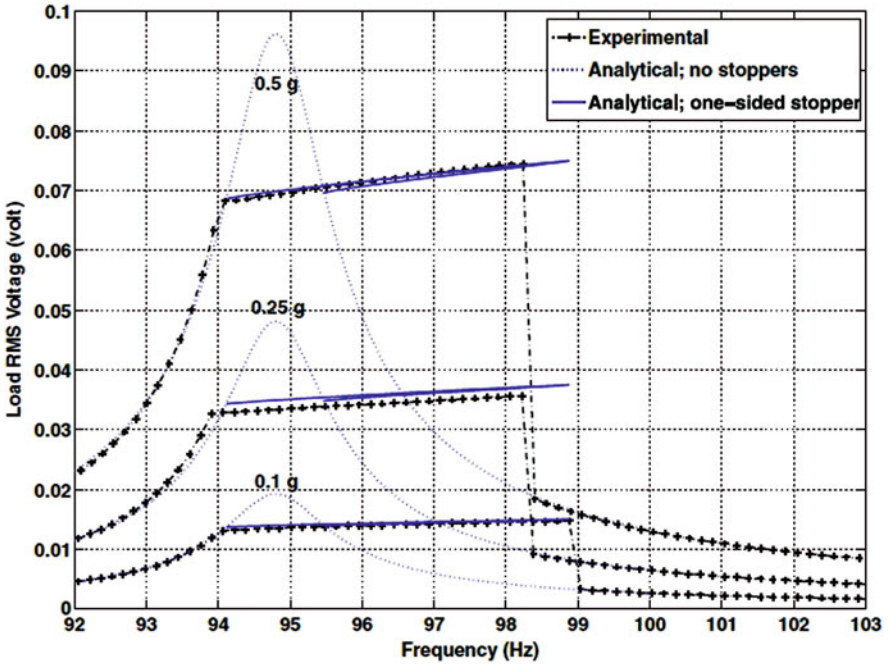

Fig. 1.70 Voltage on load versus excitation frequency [82]

$$m \cdot \frac{d^2 z\,(t)}{dt^2} + b \cdot \frac{dz\,(t)}{dt} + k \cdot z\,(t) + k_n [z(t)]^3 = -m \cdot \frac{d^2 y\,(t)}{dt^2} \tag{1.73}$$

where the spring force is the combination of linear force,

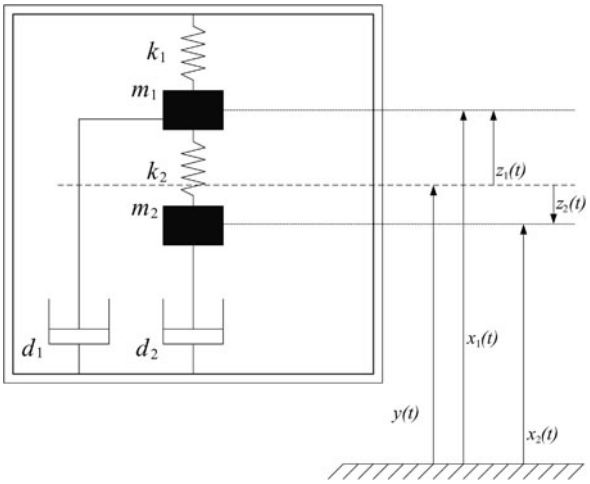

Fig. 1.71 Schematic model of a coupled oscillator [84]

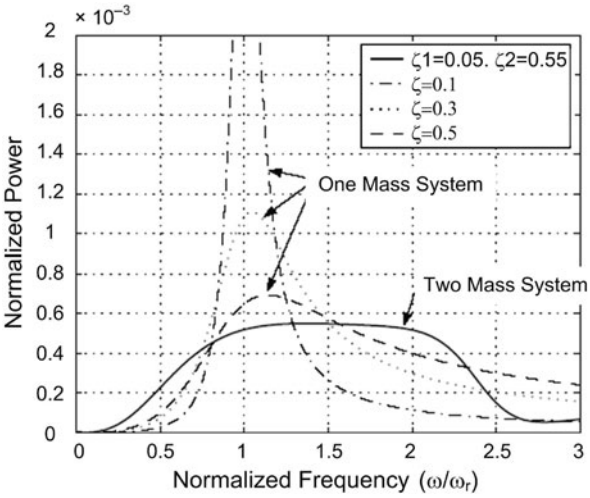

Fig. 1.72 Power spectrum for optimized two-mass system and for equivalent one-mass system with various ζ values [84]

$$\Omega_a = \sqrt{\frac{3}{4}\alpha Z^2 + (1 - 2\zeta^2) - \frac{\sqrt{a^2 - 3\alpha\zeta^2 Z^4 + 4\zeta^2 Z^2(\zeta^2 - 1)}}{Z}} \tag{1.74}$$

$$\Omega_b = \sqrt{\frac{3}{4}\alpha Z^2 + (1 - 2\zeta^2) + \frac{\sqrt{a^2 - 3\alpha\zeta^2 Z^4 + 4\zeta^2 Z^2(\zeta^2 - 1)}}{Z}} \tag{1.75}$$

where α is proportional to the non-linear spring factor, k_n, Z is the amplitude of the proof mass, ζ is the damping factor and a is the normalized excitation acceleration.

Such devices have a hardening spring which has the effect of shifting the resonant frequency. Numerical and analytical studies showed that a device with a hardening spring has a larger bandwidth over which power can be harvested due to the shift in the resonance frequency. Analytical results also showed that the bandwidth of the hardening system depends on the damping ratio, the non-linearity and the input acceleration (Fig. 1.73). Ideally, the maximum amount of power harvested by a non-linear system with a hardening stiffness is the same as the maximum power harvested by a linear system. The maximum power occurs at a different frequency depending on the non-linearity. It is important to mention that the output power and bandwidth of the non-linear generators depend on the direction of approach of the vibration frequency to the resonant frequency. For a hard non-linearity, bandwidth only increases when approaching the device-resonant frequency from a lower frequency while for a soft non-linearity, bandwidth only increases when approaching the device-resonant frequency from a higher frequency. It is unlikely that these conditions can be guaranteed in real applications.

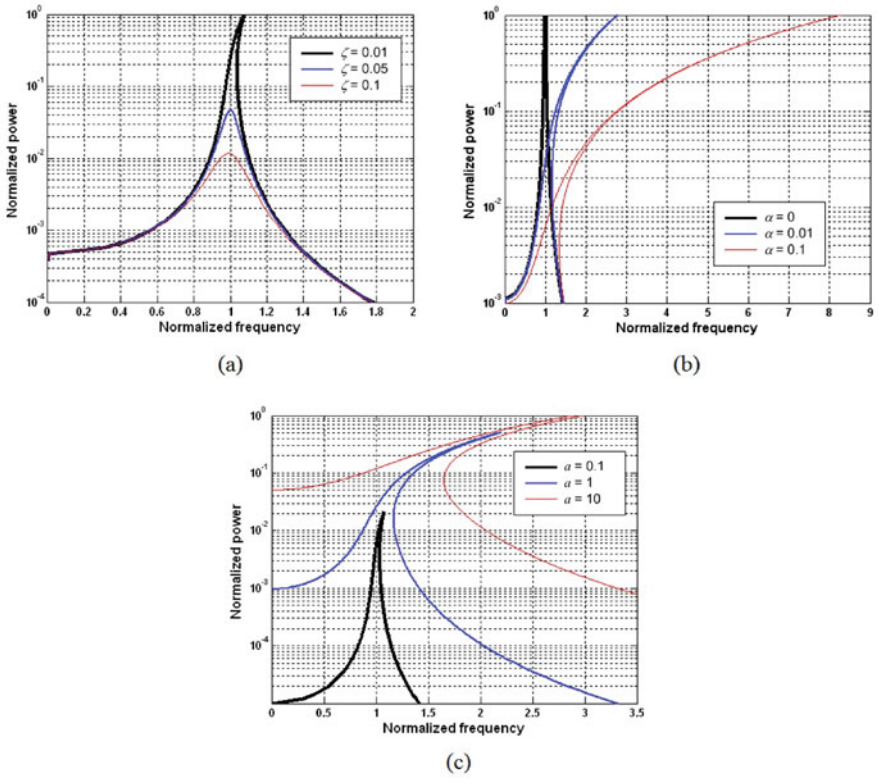

Fig. 1.73 Power spectrum of non-linear generators: (**a**) various damping ratio; (**b**) various non-linearity; and (**c**) various input acceleration

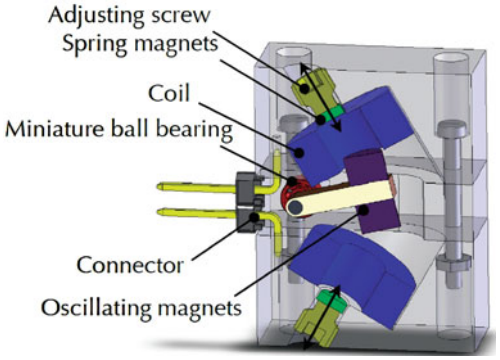

Fig. 1.74 Half-section of the device [86]

Non-linear generators can be realized by replacing using a conventional spring with a magnetic spring. Spreemann et al. [86] reported a tunable electromagnetic vibration energy harvester with a magnetic spring, which combined a tuning mechanism with the non-linear structure. Instead of using a linear suspension, this device was implemented using a rotary suspension (Fig. 1.74). The use of magnetic spring magnets resulted in a non-linear restoring force. As shown experimentally in Fig. 1.75, the resonant frequency shifted by about 30 Hz for a displacement of 1.5 mm of each spring magnet. The maximum output decreased with the increase of the magnet spacing, i.e. as the resonant frequency decreased. Also the bandwidth of the device increased as the space between magnets became smaller, i.e. non-linearity increased. This agrees with the analysis result shown in Fig. 1.73. The generator has a volume of approximately 2.5 cm^3.

In addition, the design and analysis of an energy harvesting device with magnetic restoring forces to levitate an oscillating centre magnet was presented by Mann and Sims [87]. Figure 1.76 shows the schematic diagram of the device. The device has two magnets that were mechanically attached to the generator housing. A centre magnet was placed between the two fixed magnets and the magnetic poles were oriented to repel the centre magnet, thus suspending the centre magnet with a non-linear restoring force. The non-linearity allows the linear resonance to be tuned by simply changing the spacing between outer and centre magnets.

It was found theoretically and experimentally that the response for both linear and non-linear systems scales almost linearly within some regimes of excitation amplitudes (Fig. 1.77a). However, once the non-linearities have been sufficiently engaged, as shown in Fig. 1.77b, the peak response of the non-linear system does not occur at its linear resonant frequency. In the frequency response for the non-linear system, relatively large amplitudes persist over a much larger range of frequencies, which could prove beneficial for applications with either fixed or varying excitation inputs. Furthermore, the maximum output power of such devices is delivered to the electrical load at a frequency away from linear resonance.

Burrow et al. [88, 89] reported a non-linear generator that consisted of a linear spring with the non-linearity caused by the addition of magnetic reluctance

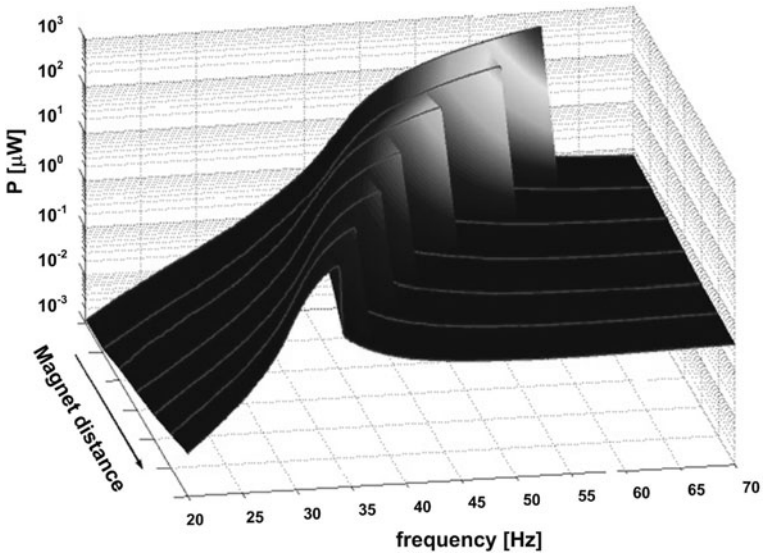

Fig. 1.75 Measured output power [86]

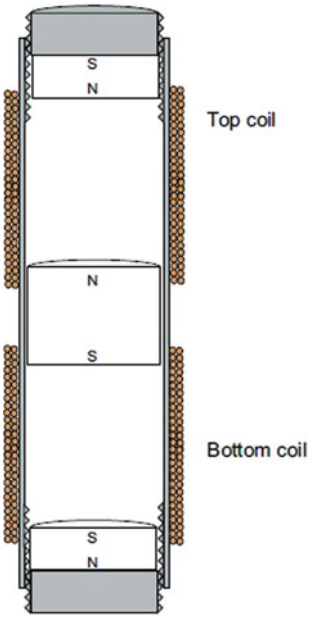

Fig. 1.76 Schematic diagram of magnetically levitated generator [87]

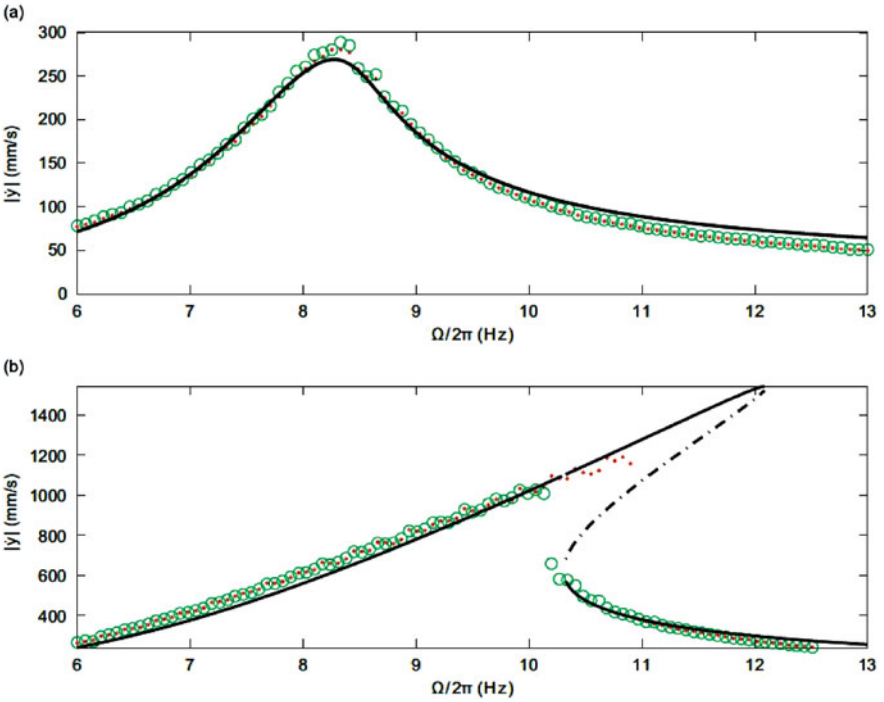

Fig. 1.77 Experimental velocity response amplitudes from forward (*dots*) and reverse frequency sweeps (*circles*) are compared with theory. Theoretical predictions are separated into stable solutions (*solid line*) and unstable solutions (*dashed line*): (**a**) Excitation level of m s^{-2} (**b**) excitation level of 8.4 and m s^{-2} [87]

forces. Figure 1.78 shows the schematic diagram of the non-linear generator. The flux concentrator guides the magnetic flux through the coil. The vibration of the magnets causes a change in direction of the magnetic flux, which induces a voltage across the coil. The reluctance force between the magnets and the flux concentrator resulted in the non-linearity. It is found experimentally that the generator has a wider bandwidth during an up-sweep, i.e. when the excitation frequency was gradually

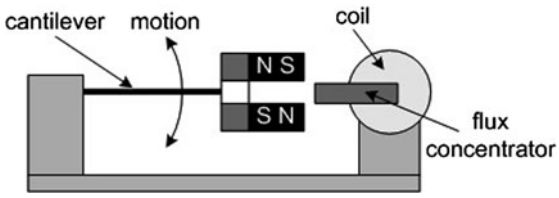

Fig. 1.78 Schematic diagram of a non-linear generator (after [89])

increased while the bandwidth was much narrower during a down-sweep, i.e. when the excitation frequency was gradually decreased.

Tvedt et al. [90] studied non-linear behaviour in an electrostatic vibration energy harvester. The measured non-linear phenomena were described by a lumped model with a non-linear beam displaying both spring softening and hardening. Experimental results show that considerable bandwidth enhancements can be achieved by using non-linear springs without relying on mechanical stopper impacts, resonance tuning or large electromechanical coupling.

1.6.5 Bi-stable Generators

Ramlan et al. [85] studied a bi-stable structure for energy harvesting (also termed the snap-through mechanism). These structures employ a negative stiffness which has the effect of steepening the displacement response of the resonator as a function of time resulting in a higher velocity for a given input excitation. Analysis revealed that the amount of power harvested by a bi-stable device is $4/\pi$ greater than that of the tuned linear device provided the device produces a square wave output for a given sinusoidal input. Numerical results also showed that more power is harvested by the mechanism if the excitation frequency is much less than the generator's resonant frequency. Although the bi-stable mechanism cannot produce a square wave like response under all operating conditions, it offers better performance than the linear mechanism at lower frequencies than the resonant frequency of the linear device. Bi-stable devices also have the potential to cope with mismatch between resonant frequency and vibration frequency.

Galchev et al. [91] reported an electromagnetic generator with a bi-stable structure for scavenging low-frequency non-periodic vibrations. The bi-stable mechanical structure is used to initiate high-frequency mechanical oscillations in an electromagnetic transducer. The fabricated device generated a peak power of 288 μW and an average power of 5.8 μW from an input acceleration of 9.8 m s^{-2} at 10 Hz. The device operates over a frequency range of 20 Hz. The internal volume of the generator is 2.1 cm^3 (3.7 cm^3 including casing), half of a standard AA battery.

Mann and Owens [92] investigated a non-linear energy harvester that uses magnetic interactions to create an inertial generator with a bi-stable potential well. Both theoretical and experimental results show that the potential well escape phenomenon can be used to broaden the frequency response of an energy harvester.

Both Ferrari et al. [93] and Stanton et al. [94] studied the bi-stable structure as shown in Fig. 1.79. Both generators have piezoelectric cantilevers and were tested in vibration with random frequencies. Their experimental results show that bi-stable structure can increase output power of the generator in a wider frequency range.

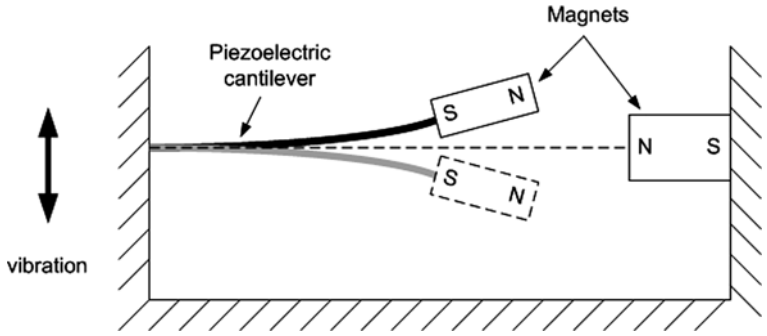

Fig. 1.79 A bi-stable piezoelectric cantilever

1.7 Comparisons of Different Strategies for Adaptive Kinetic Energy Harvesting

It has been proven theoretically and experimentally that both tuning resonant frequency and widening the bandwidth of kinetic energy harvesters can increase their operational frequency range.

To compare the performance of a single generator with a wide bandwidth, a generator array and a single tunable generator with constant damping, typical specifications of these three types of generators have been chosen. G1, G2 and G3, listed in Table 1.7, represent a single generator with a wide bandwidth, a generator array and a single tunable generator with constant damping, respectively. Figure 1.80 shows the comparison of power spectra of these three types of generator.

Table 1.7 List of specifications in Fig. 1.80

Figure	1.80a	1.80b	1.80c	1.80d
Operational frequency range	90.5–110.5%	90.5–110.5%	61–160.5%	61–160.5%
Q-factor of G1	5	5	1	1
Q-factor of G2	50	80	10	50
Number of individual generator in G2, n	14	20	33	100
Resonant frequencies of individual generators in G2	$90\%+n\times1.4\%$	$90\%+n\times1\%$	$60\%+n\times3\%$	$60\%+n\times1\%$
Q-factor of G3	110	110	160	160
Mass ratio	40:2:1	40:1.3:1	200:4:1	200:1.3:1

In Fig. 1.80a, curves 1 and 3 are both single generators. Curve 2 consists of a generator array of 14 generators of Q-factor of 50. In Fig. 1.80b, curves 1 and 3 are identical to Fig. 1.80a. Curve 2 now consists of a generator array of 20 generators of Q-factor of 80. In Fig. 1.80c, for curve 1, the Q-factor has been reduced to 1. Curve 2 shows a generator array of 33 generators of Q-factor of 10. Curve 3 has the same Q-factor as in Fig. 1.80a and b but with higher mass. In Fig. 1.80d, curves 1

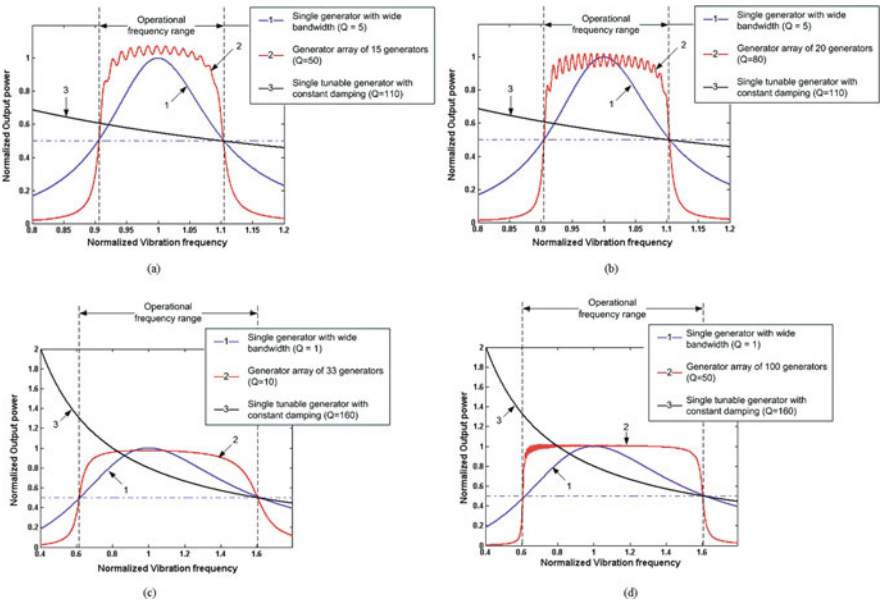

Fig. 1.80 Comparison of a single generator with a wide bandwidth, a generator array and a single tunable generator with constant damping

and 3 are identical to Fig. 1.80c. Curve 2 now consists of a generator array of 100 generators of Q-factor of 50.

When the Q-factor of a single generator decreases, its bandwidth increases. To generate the same amount of output power as the original bandwidth, a single generator has to be larger as the bandwidth increases.

If a generator array is used to widen the operational frequency range, one can design a few larger individual generators with low Q-factor with large resonant frequency gap between generators or many smaller individual generators with high Q-factor but small resonant frequency gap between generators. By contrast, it is much easier to design small tunable generators with constant damping to cover the same amount of operational frequency range at the cost of extra energy to power the frequency-tuning mechanisms.

Table 1.8 compares the advantages and disadvantages of different strategies to realize adaptive kinetic energy harvesters.

1.8 Summary

Several power supply strategies for wireless sensor networks have been introduced in this chapter. Attention has been paid especially to vibration-based microgenerators. A particular transduction mechanism is used to extract electrical energy

Table 1.8 Comparisons of different strategies

Strategies	Advantages	Disadvantages
Mechanical tuning	• High efficiency	○ Extra system and energy are required ○ Responds to only one frequency at a time ○ Slow response to change in vibration frequency
◇ Change dimension	• Does not affect damping	○ Difficult to implement ○ Not suitable for tuning in situ[a]
◇ Change centre of gravity	• Does not affect damping	○ Not suitable for tuning in situ
◇ Change spring stiffness continuously	• Suitable for in situ tuning	○ Consumes energy when generators work at resonance
◇ Apply axial load (change spring stiffness intermittently)	• Easy to implement • Suitable for in situ tuning • No energy is required when generators work at resonance • Damping is not affected when tensile load is applied	○ Increased damping when compressive load is applied
Electrical tuning	• Easy to implement • No energy is required when generators work at resonance • Suitable for in situ tuning	○ Low tuning efficiency ○ Complexity in designing the generator
Widen bandwidth	• No tuning mechanism required • Respond to different frequencies at the same time • Immediate response to change in vibration frequency	○ Complexity in design
◇ Generator array	• Damping is not affected	○ Complexity in design ○ Low volume efficiency
◇ Use mechanical stopper	• Easy to implement	○ Fatigue problem ○ Decrease in maximum output power
◇ Coupled oscillators	• Easy to implement	○ Decrease in maximum output power
◇ Non-linear generators	• Better performance at excitation frequencies higher than resonant frequency	○ Complexity in design ○ Hysteresis
◇ Bi-stable structure	• Better performance at excitation frequencies much lower than resonant frequency	○ Complexity in design

[a]In situ tuning: Tuning while the generator is mounted on the vibration source and working

from motion. The main transduction mechanisms are electromagnetic, electrostatic, piezoelectric and magnetostrictive.

Equation (1.21) gives a good guideline in designing kinetic energy harvesters. It is found that the maximum power converted from the mechanical domain to the electrical domain is proportional to the mass and vibration acceleration and inversely proportional to resonant frequency as well as mechanical (electrical) damping factor. This means that more power can be extracted if the inertial mass is increased or the generator can work in the environment where the vibration level is high. For a fixed resonant frequency, the generator has to be designed to make the mechanical damping as small as possible. For a generator with constant mechanical damping, the generated electrical power drops with an increase of the resonant frequency.

As most practical applications for kinetic energy harvesters exhibit frequency variations over time, it is not possible to guarantee that fixed frequency generators will always work at resonance and produce maximum output power. Mechanisms have to be employed to increase the operational frequency range of kinetic energy harvesters. Therefore, adaptive kinetic energy harvesters are developed. Generally, there are two possible solutions to adaptive kinetic energy harvesting. One is to tune the resonant frequency of a single generator and the other is to widen the bandwidth of the generator.

To tune the resonant frequency of a single generator, a certain mechanism has to be employed to periodically adjust the resonant frequency to match the frequency of ambient vibration at all times. Maximum power can then be generated at various frequencies without reducing the Q-factor and with high efficiency per unit volume. Tuning mechanisms can be classified as intermittent tuning and continuous tuning. Intermittent tuning has advantages over continuous tuning; in intermittent tuning, mechanism is turned off when the generator operates at the desired frequency thereby consuming negligible energy, which makes producing a net output power more probable. There are two methods to tune the resonant frequency: mechanical tuning and electrical tuning.

Among mechanical methods of frequency tuning, changing the dimensions of the structure and the position of the centre of gravity are potentially suitable for intermittent tuning. However, it is problematic to change and maintain the new dimensions of the structure or the centre of gravity of the proof mass during operation. The most suitable approach to changing the dimensions of the structure is to change its length. This requires that the structure clamp is removed, the length adjusted and then the structure re-clamped. If the structure cannot be clamped properly after tuning finishes, the performance of the generator will be severely affected by introducing damping effects through the supports. To change the position of the centre of gravity of the mass during operation, an actuator has to be embedded in the mass, which increases the complexity of the device. Therefore, these two methods are not suitable for in situ tuning (tuning while the generator is mounted on the vibration source and working) or tuning with automatic control.

Alternatively the frequency can be tuned by changing the spring stiffness intermittently or continuously. They are both suitable for in situ tuning but intermittently

changing the spring stiffness is always preferred for efficiency reasons. However, extra systems and energy are required to realize tuning using mechanical methods.

It is important to mention that the efficiency of mechanical tuning methods also depends on the size of the structure. The smaller the resonator, the higher the efficiency of the tuning mechanism.

Resonant frequency tuning by adjusting the electrical load has been practically shown to be feasible. This method consumes little energy as it does not involve any change in mechanical properties. Energy is only consumed in electronic switches and control unit, which is typically far less than that consumed in mechanical tuning methods. In addition, it is much easier to be implemented than mechanical methods. However, the tuning efficiency of electrical tuning method to date is quite low and this method cannot achieve a large tuning range. It is a more suitable method when tunable frequency range required is small. An extra closed-loop system also has to be introduced to control the tuning process.

It is concluded that when choosing frequency method for a certain application, following factors need to be taken into consideration:

- The energy consumed by the tuning mechanism should be as small as possible and must not exceed the energy produced by the generator.
- The mechanism should achieve a sufficient operational frequency range.
- The tuning mechanism should achieve a suitable degree of frequency resolution.
- The generator should have as high as possible Q-factor to achieve maximum power output and the strategy applied should not increase the damping, i.e. decrease Q-factor, over the entire operational frequency range.

For the second solution, i.e. to widen the bandwidth, there is a trade-off between the system bandwidth and the Q-factor. Wider bandwidth means, for a single resonator, a lower Q-factor, which reduces the maximum output power. Bandwidth can also be effectively widened by designing a generator consisting of an array of small generators, each of which works at a different frequency. Thus, the assembled generator has a wide operational frequency range while the Q-factor does not decrease. However, this assembled generator must be carefully designed so that each individual generator does not affect the others. This makes it more complex to design and fabricate. Additionally, at a particular vibration frequency, only a single or a few individual generators contribute to power output so the approach is volume inefficient.

Another method used to increase the bandwidth is to use an amplitude limiter to limit the amplitude of the resonator. The drawbacks are that this method causes the maximum output power to drop by limiting vibration amplitude and the repeating mechanical contact between the cantilever and the mechanical stopper may result in earlier fatigue-induced failure in the cantilever beam.

Employing a coupled oscillator can also increase the operational bandwidth of the generator. It can achieve flat response over a wide frequency range. However, the maximum output power of a coupled oscillator generator is significantly lower than a generator with a single mass.

Furthermore, non-linear generators and generators with bi-stable structures are two further potential solutions to increase the operational frequency range of kinetic energy harvesters. They can improve performance of the generator at higher and lower frequency bands relative to its resonant frequency, respectively. However, the mathematical modelling of these generators is more complicated than that of linear generators, which increases the complexity in design and implementation. Besides, there is hysteresis in non-linear generators. Performance during down-sweep (or up-sweep) can be worse than that during up-sweep (or down-sweep) or worse than the linear region depending on sweep direction as explained in Section 1.6.

In conclusion, for vibration energy harvesting, possible strategies to increase the operation frequency range include

- changing spring stiffness intermittently (preferred) or continuously;
- straining the structure intermittently (preferred) or continuously;
- adjusting capacitive load;
- using generator array; and
- employing non-linear and bi-stable structures.

To realize these strategies properly, the following issues have to be considered. For intermittent mechanical tuning, the tuning system has to be designed to consume as little energy as possible and not to affect the damping so as to make the generator harvest maximum power. In addition, currently commercially available linear actuators are still large in size compared to millimetre-scale micro-generator. To keep tunable generators of reasonable size, it is important to use miniature actuators. Generators capable of electrical tuning must have strong electromechanical coupling to enable larger tuning ranges. Moreover, theoretical analyses of non-linear generators and generators with bi-stable structures have not been sufficiently developed and further attention should be paid to practically implement them.

Kinetic energy harvesting has been well studied in the past decade. It has been regarded as one of the best alternatives to energy source for wireless sensor networks. However, its drawback of narrow operational frequency bandwidth severely limits its application. With the recent development of adaptive kinetic energy harvesting, this drawback will eventually overcome, which will bring kinetic energy harvesting to much broader applications.

References

1. Roundy S, Wright PK, Rabaey J (2003) A study of low level vibrations as a power source for wireless sensor nodes. Comp. Comm. 26: 1131–1144
2. Beeby SP, Tudor MJ, White NM (2006) Energy harvesting vibration sources for microsystems applications. Meas. Sci. Tech. 17: 175–195
3. Zhu D, Tudor MJ, Beeby SP (2010) Strategies for increasing the operating frequency range of vibration energy harvesters: a review. Meas. Sci. Tech. 21(2): 022001
4. Williams CB, Yates RB (1996) Analysis of a micro-electric generator for microsystems. Sens. Actuator A 52: 8–11

5. Arnold DP (2007) Review of microscale magnetic power generation. IEEE Tran. Mag. 43(11): 3940–3951
6. Roundy S, Wright P, Pister K (2002) Micro-electrostatic vibration-to-electricity converters. Proceedings of IMECE, 1–10
7. Sodano HA, Inman DJ, Park G (2004) A review of power harvesting from vibration using piezoelectric materials. Shoock Vibr. Dig. 36(3): 197–205
8. Beeby SP, Tudor MJ, Torah RN, Roberts S, ODonnell T, Roy S (2007) Experimental comparison of macro and micro scale electromagnetic vibration powered generators. Microsyst. Tech. 13: 1647–1653
9. Stephen NG (2006) On energy harvesting from ambient vibration. J. Sound Vibr. 293: 409–25
10. Williams CB, Shearwood C, Harradine MA, Mellor PH, Birch TS, Yates RB (2001) Development of an electromagnetic micro-generator. IEE Proc. Circuits Dev. Syst. 148: 337–342
11. Ching NNH, Wong HY, Li WJ, Leong PHW, Wen Z (2002) A laser-micromachined vibrational to electrical power transducer for wireless sensing systems. Sens. Actuator A 97–98: 685–690
12. Glynne-Jones P, Tudor MJ, Beeby SP, White NM (2004) An electromagnetic, vibration-powered generator for intelligent sensor systems. Sens. Actuator A 110: 344–349
13. Koukarenko E, Beeby SP, Tudor MJ, White NM, ODonnell T, Saha T, Kulkani S, Roy S (2006) Microelectromechanical systems vibration powered electromagnetic generator for wireless sensor applications. Microsys. Tech. 12 (11): 1071–1077
14. Saha CR, ODonnell T, Loder H, Beeby SP, Tudor MJ (2006) Optimization of an electromagnetic energy harvesting device. IEEE Trans. Magnetics 42(10): 3509–3511
15. Beeby SP, Torah RN, Tudor MJ, Glynne-Jones P, ODonnell T, Saha CR, Roy S (2006) A micro electromagnetic generator for vibration energy harvesting. J. Micromech. Microeng. 17: 1257–65
16. Klahand H, Najafi K (2008) Energy scavenging from low-frequency vibrations by using frequency up-conversion for wireless sensor applications. IEEE Sensors J. 8(3): 261–268
17. Torah RN, Glynne-Jones P, Tudor MJ, ODonnell T, Roy S, Beeby SP (2008) Self-powered autonomous wireless sensor node using vibration energy harvesting. Meas. Sci. Tech. 19: 125202
18. Wang P, Dai X, Zhao X, Ding G (2009) A micro electromagnetic vibration energy harvester with sandwiched structure and air channel for high energy conversion efficiency. Proceedings of PowerMEMS 2009, Washington, DC, 296–299
19. Anton SR, Sodano HA (2007) A review of power harvesting using piezoelectric materials (2003–2006). Smart Mater. Struct. 16: 1–21
20. Sodano HA, Inman DJ (2005) Comparison of piezoelectric energy harvesting devices for recharging batteries. J. Intell. Mater. Syst. Struct. 16(10): 799–807
21. Roundy S, Wright PH, Rabaey JM (2004) Energy Scavenging for Wireless Sensor Networks with Special Focus on Vibrations. Kluwer, Norwell, MAs
22. MEMSnet http://www.memsnet.org/material.Cited18May2010
23. White NM, Glynne-Jones P, Beeby SP (2001) A novel thick-film piezoelectric micro-generator. Smart Mater. Struct. 10: 850–852
24. Lu F, Lee HP, Lim SP (2004) Modeling and analysis of micro piezoelectric power generators for micro-electromechanical-systems applications. Smart Mater. Struct. 13: 57–63
25. Jeon YB, Sood R, Jeong J-h, Kim SG (2005) MEMS power generator with transverse mode thin film PZT. Sens. Actuator A 122: 16–22
26. Fang HB, Liu J-Q, Xu ZY, Dong L, Wang L, Chen D, Cai BC, Liu Y (2006) Fabrication and performance of MEMS-based piezoelectric power generator for vibration energy harvesting. Microelectronics J. 37: 1280–1284
27. Marzencki M, Ammar Y, Basrour S (2007) Integrated power harvesting system including a MEMS generator and a power management circuit. Sens. Actuator. A 145–146: 363–370
28. Jeong S-J, Kim M-S, Song J-S, Lee H-K (2008) Two-layered piezoelectric bender device for micro-power generator. Sens. Actuator A 148: 158–167

29. Kok SW, White NW, Harris NH (2008) A novel piezoelectric thick-film free-standing cantilever energy harvester. EUROSENSORS XXII, Dresden, Germany, 395–399
30. Shen D, Park J-H, Ajitsaria J, Choe S-Y, Wikle III HC, Kim DJ (2008) The design, fabrication and evaluation of a MEMS PZT cantilever with an integrated Si proof mass for vibration energy harvesting. J. Micromech. Microeng. 18: 055017
31. Zhu D, Beeby SP, Tudor MJ, Harris NR (2009) A self powered smart tag for wireless structure health monitoring in aeronautical applications. Proceedings of PowerMEMS 2009, Washington, DC, 201–204
32. Meninger S (1999) A low power controller for a MEMS based energy converter. MSc thesis, MIT, USA
33. Mitcheson PD, Green TC, Yeatman EM, Holmes AS (2004) Architectures for vibration-driven micropower generators., IEEE J. Microelectromech. Syst. 13: 429–440
34. Meninger S, Mur-Miranda J, Lang J, Chandrakasan A, Slocum A, Schmidt M, Amirtharajah R (2001) Vibration to electric energy conversion. IEEE Trans. VLSI Syst. 9: 64–76
35. Tashiro R, Kabei N, Katayama K, Tsuboi F, Tsuchiya K (2002) Development of a electrostatic generator for a cardiac pacemaker that harnesses the ventricular wall motion. J. Artif. Organs 5(4): 239–45
36. Mitcheson P, Stark B, Miao P, Yeatman E, Holmes A, Green T (2003) Analysis and optimisation of MEMS on-chip power supply for self powering of slow moving sensors. Eurosensors 03, 17th European conference on sensors and actuators, University of Minho, Guimaraes, Portugal, 48–51
37. Arakawa Y, Suzuki Y, Kasagi N (2004) Micro seismic power generator using electret polymer film. Proceedings of PowerMEMS 2004, Kyoto, Japan, 187–190
38. Despesse G, Jager T, Chaillout J, Leger J, Vassilev A, Basrour S, Chalot B (2005) Fabrication and characterisation of high damping electrostatic micro devices for vibration energy scavenging. Proceedings of Design, Test, Integration and Packaging of MEMS and MOEMS. 386–390
39. Kuehne I, Frey A, Eckstein G, Schmid U, Seidel Haging (2006) Design and analysis of a capacitive vibration-to-electrical energy converter with built-in voltage. Proceedings of the 36th European Solid-State Device Research Conference 138–141
40. Yen BC, Lang JH (2006) A variable-capacitance vibration-to-electric energy harvester. IEEE Trans. Circuits Syst.-I: Regular Papers 53(2): 288–295
41. Sterken T, Fiorinil P, Altena G, Van Hoof C, Puers R (2007) Harvesting energy from vibrations by a micromachined electret generator. International Solid-State Sensors, Actuators and Microsystems Conference, Lyon, France, 129–132
42. Lo H, Tai YC (2008) Parylene-based electret power generators. J. Micromech. Microeng. 18: 104006
43. Hoffmann D, Folkmer B, Manoli Y (2009) Fabrication, characterization and modelling of electrostatic micro-generators. J. Micromech. Microeng. 19: 094001
44. Naruse Y, Matsubara N, Mabuchi K, Izumi M, Suzuki S (2009) Electrostatic micro power generation from low-frequency vibration such as human motion. J. Micromech. Microeng. 19: 094002
45. Huang J, O'Handley RC, Bono D (2003) New, high-sensitivity, hybrid magnetostrictive/electroactive magnetic field sensors. Proceedings of the SPIE 5050. 229–237
46. Wang L, Yuan FG (2008) Vibration energy harvesting by magnetostrictive material. Smart Mater. Struct. 17: 045009
47. Dai X, Wen Y, Li P, Yang J, Zhang G (2009) Modeling, characterization and fabrication of vibration energy harvester using Terfenol-D/PZT/Terfenol-D composite transducer. Sens. Actuator A 156: 350–358
48. Roundy S (2005) On the effectiveness of vibration-based energy harvesting. J. Intell. Mater. Syst. Struct. 16: 809–823
49. Mide Technology. http://www.mide.com/.Cited21May2010
50. Perpetuum Ltd. http://www.perpetuum.com/.Cited21May2010

51. Blevins RD (2001) Formulas for natural frequency and mode shape. Krieger, New York, NY
52. Gieras JF, Oh J-H, Huzmezan M, Sane HS (2007) Electromechanical energy harvesting system. Patent publication number: WO2007070022 (A2), WO2007070022 (A3)
53. Roylance L, Angell JB (1979) A batch fabricated silicon accelerometer. IEEE Trans. Electron Dev. 26(12): 1911–1917
54. Wu X, Lin J, Kato S, Zhang K, Ren T, Liu L (2008) A frequency adjustable vibration energy harvester. Proceedings of PowerMEMS 2008, Sendai, Japan, 245–248
55. Scheibner D, Mehner J, Reuter D, Kotarsky U, Gessner T, Dtzel W (2004) Characterization and self-test of electrostatically tunable resonators for frequency selective vibration measurements. Sen. Actuator. A 111: 93–99
56. Scheibner D, Mehner J, Reuter D, Gessner T, Dtzel W (2005) A spectral vibration detection system based on tunable micromechanical resonators. Sens. Actuator A 123–124: 63–72
57. Adams SG, Bertscht FM, Shawt KA, Hartwell PG, MacDonald NC, Moon FC (1995) Capacitance based tunable micromechanical resonators. The 8th International Conference on Solid-State Sensors and Actuators, and Eurosensors IX, Stockholm, Sweden, 438–441
58. Lee KB, Lin L, Cho YH (2008) A closed-form approach for frequency tunable comb resonators with curved finger contour. Sens. Actuator A 141: 523–529
59. Piazza G, Abdolvand R, Ho GK, Ayazi F (2004) Voltage-tunable piezoelectrically transduced single-crystal silicon micromechanical resonators. Sens. Actuator A 111: 71–78
60. Yao JJ, MacDonald NC (1996) A micromachined, single-crystal silicon, tunable resonator. J. Micromech. Microeng. 6: 257–264
61. Thiesen J, O'Brian GP (2006) Energy harvester with adjustable resonant frequency. Patent publication number: WO2006046937 (A1), EP1803170 (A1), US2008129147 (A1), EP1803170 (A0), CN101002343 (A)
62. Peters C, Maurath D, Schock W, Mezger F, Manoli Y (2009) A closed-loop wide-range tunable mechanical resonator for energy harvesting systems. J. Micromech. Microeng. 19: 094004
63. Wischke M, Masur M, Goldschmidtboeing F, Woias P (2010) Electromagnetic vibration harvester with piezoelectrically tunable resonance frequency. J. Micromech. Microeng. 20: 035025
64. Challa VR, Prasad MG, Shi Y, Fisher FT (2008) A vibration energy harvesting device with bidirectional resonance frequency tunability. Smart Mater. Struct. 17: 015035
65. Remtema T, Lin L (2001) Active frequency tuning for micro resonators by localized thermal stressing effects. Sens. Actuator A 91: 326–332
66. Syms RRA (1998) Electrothermal frequency tuning of folded and coupled vibrating micromechanical resonators. J. Microelectromechan. Syst. 7(2): 164–171
67. Cabuz C, Fukatsu K, Hashmoto H, Shoji S, Kurabayashi T, Minami K, Esashi M (1994) Fine frequency tuning in resonant sensors. Proceedings of IEEE Workshop on MEMS, Oiso, Japan, 245–250
68. Leland ES, Wright PK (2006) Resonance tuning of piezoelectric vibration energy scavenging generators using compressive axial preload. Smart Mater. Struct. 15: 1413–1420
69. Mukherjee R (2007) MEMS resonator using frequency tuning. Patent publication number: US20070214890A1
70. Hu Y, Xue H, Hu H (2007) A piezoelectric power harvester with adjustable frequency through axial preloads. Smart Mater. Struct. 16: 1961–1966
71. Eichhorn C, Goldschmidtboeing F, Woias P (2009) Bidirectional frequency tuning of a piezoelectric energy converter based on a cantilever beam. J. Micromech. Microeng. 19: 094006
72. Zhu D, Roberts S, Tudor MJ, Beeby SP (2008) Closed loop frequency tuning of a vibration-based micro-generator. Proceedings of PowerMEMS, Sendai, Japan, 229–232
73. Zhu D, Roberts S, Tudor MJ, Beeby SP (2009) Design and experimental characterisation of a tunable vibration-based electromagnetic micro-generator. Sens. Actuator A 158(2): 284–293
74. Wu W-J, Chen Y-Y, Lee B-S, He J-J, Peng Y-T (2006) Tunable resonant frequency power harvesting devices. Proc. of SPIE 6169: 55–62

75. Charnegie D (2007) Frequency tuning concepts for piezoelectric cantilever beams and plates for energy harvesting. MSc Dissertation School of Engineering, University of Pittsburgh, Pittsburgh, PA
76. Cammarano A, Burrow SG, Barton DAW, Carrella A, Clare LR (2010) Tuning a resonant energy harvester using a generalized electrical load. Smart Mater. Struct. 19: 055003
77. Xue H, Hu Y, Wang Q-M (2008) Broadband piezoelectric energy harvesting devices using multiple bimorphs with different operating frequencies. IEEE Trans. Ultrason. Ferroelectr. Freq. Control 55(9): 2104–2108
78. Feng G-H, Hung J-C (2007) Optimal FOM designed piezoelectric microgenerator with energy harvesting in a wide vibration bandwidth. Proceedings of the 2nd IEEE International Conference on Nano/Micro Engineered and Molecular Systems, Bangkok, Thailand, 511–514
79. Ferrari M, Ferrari V, Guizzetti M, Marioli D, Taroni A (2008) Piezoelectric multifrequency energy converter for power harvesting in autonomous microsystems. Sens. Actuator A 142: 329–335
80. Sari I, Balkan T, Kulah H (2007) A wideband electromagnetic micro power generator for wireless microsystems International Solid-State. Sensors, Actuators and Microsystems Conference, Lyon, France, 275–278
81. Lin SC, Lee BS, Wu WJ, Lee CK (2009) Multi-cantilever piezoelectric MEMS generator in energy harvesting. IEEE Int. Ultrason. Symp. Proc. 755–758
82. Soliman MSM, Abdel-Rahman EM, El-Saadany EE, Mansour RR (2008) A wideband vibration-based energy harvester. J. Micromech. Microeng. 18: 115021
83. Soliman MSM, Abdel-Rahman EM, El-Saadany EE, Mansour RR (2009) A design procedure for wideband micropower generators. J. MEMS. 18(6): 1288–1299
84. Petropoulos T, Yeatman EM, Mitcheson PD (2004) MEMS coupled resonators for power generation and sensing. Micromechanics Europe, Leuven, Belgium
85. Ramlan R, Brennan MJ, Mace BR, Kovacic I (2010) Potential benefits of a non-linear stiffness in an energy harvesting device. Nonlin. Dyn. 59: 545–558
86. Spreemann D, Folkmer B, Maurath D, Manoli Y (2006) Tunable transducer for low frequency vibrational energy scavenging. Proceedings of EurosensorsXX, Göteborg, Sweden
87. Mann BP, Sims ND (2009) Energy harvesting from the nonlinear oscillations of magnetic levitation. J. Sound Vibr. 319: 515–530
88. Burrow SG, Clare LR (2007) A resonant generator with non-linear compliance for energy harvesting in high vibrational environments. IEMDC '07 1: 715–720
89. Burrow SG, Clare LR, Carrella A, Barton D (2008) Vibration energy harvesters with non-linear compliance. Proc. of SPIE. 6928: 692807
90. Tvedt LGW, Nguyen DS, Halvorsen E (2010) Nonlinear behavior of an electrostatic energy harvester under wide- and narrowband excitation. J. MEMS 19(2): 305–316
91. Galchev T, Kim H, Najafi K (2009) A parametric frequency increased power generator for scavenging low frequency ambient vibrations. Eurosensors XXIII Conference Procedia Chemistry 1: 1439–1442
92. Mann BP, Owens BA (2010) Investigations of a nonlinear energy harvester with a bistable potential well. J. Sound and Vibr. 329: 1215–1226
93. Ferrari M, Ferrari V, Guizzetti M, Ando B, Baglio S, Trigona C (2009) Improved energy harvesting from wideband vibrations by nonlinear piezoelectric Converters. Eurosensors XXIII Conference Procedia Chemistry 1: 1203–1206
94. Stanton SC, McGehee CC, Mann BP (2010) Nonlinear dynamics for broadband energy harvesting: Investigation of a bistable piezoelectric inertial generator. Physica D 239: 640–653